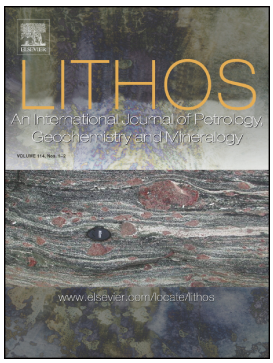

Mineralogical and geochemical study of rodingites and associated serpentinized peridotite, Eastern Desert of Egypt, Arabian-Nubian Shield

Heba S. Mubarak, Mokhles K. Azer, Adel A. Surour, Hilmy E. Moussa, Paul D. Asimow, Mona Kabesh

PII: S0024-4937(20)30357-1

DOI: https://doi.org/10.1016/j.lithos.2020.105720

Reference: LITHOS 105720

To appear in: *LITHOS*

Received date: 27 June 2020

Revised date: 28 July 2020

Accepted date: 28 July 2020

Please cite this article as: H.S. Mubarak, M.K. Azer, A.A. Surour, et al., Mineralogical and geochemical study of rodingites and associated serpentinized peridotite, Eastern Desert of Egypt, Arabian-Nubian Shield, *LITHOS* (2020), https://doi.org/10.1016/j.lithos.2020.105720

Mineralogical and geochemical study of rodingites and associated serpentinized peridotite, Eastern Desert of Egypt, Arabian-Nubian Shield

By

Heba S. Mubarak[1], Mokhles K. Azer[1], Adel A. Surour[2], Hilmy E. Moussa[1], Paul D. Asimow[3], Mona Kabesh[2]*

[1]*Geological Sciences Department, National Research Centre, 12622-Dokki, Cairo, Egypt*

[2]*Department of Geology, Cairo University, Egypt*

[3]*Division of Geological & Planetary Sciences, California Institute of Technology, Pasadena CA 91125, USA*

Abstract

We studied rodingite and rodingite-like rocks within a serpentinized ultramafic sequence and ophiolitic mélange at Um Rashid, in the Eastern Desert of Egypt. The Um Rashid ophiolite is strongly deformed, metamorphosed, and altered by serpentinization, carbonatization, listvenitization, rodingitization and silicification. The textures, whole-rock chemistry, and composition of fresh primary mineral relics show that the serpentinite protoliths were strongly melt-depleted harzburgite and minor dunite, typical of a supra-subduction zone fore-arc setting. The light-colored rocks replacing gabbro are divided on the basis of field relations, mineral assemblages and geochemical characteristics into typical rodingite and rodingite-like rock. Typical rodingite, found as blocks with chloritite blackwall rims within ophiolitic mélange, contains garnet, vesuvianite, diopside and chlorite with minor prehnite and opaque minerals. Rodingite-like rock, found as dykes in serpentinite, consists of hercynite, preiswerkite, margarite, corundum, prehnite, ferropargasite, albite, andesine, clinozoisite and diaspore. Some rodingite-like rock samples preserve relict gabbroic minerals and texture, whereas typical rodingite is fully

[*]**Corresponding author:** Prof. Mokhles K. Azer (mokhles72@yahoo.com)

replaced. Rodingite is highly enriched in CaO, Fe_2O_3, MgO, and compatible trace elements, whereas rodingite-like rock is strongly enriched in Al_2O_3 and incompatible trace elements. Based on geochemistry and petrographic evidence, both types of rodingitic rocks likely developed from mafic protoliths in immediate proximity to serpentinite but were affected by interaction with different fluids, most likely at different times. Typical rodingite development likely accompanied serpentinization and shows mineral assemblages characteristic of low-Si, high-Ca fluid infiltration at about 300°C. Rodingite-like rock, on the other hand, likely developed from seawater infiltration.

.

Keywords: Arabian-Nubian Shield, Rodingitization, Carbonatization, garnet, vesuvianite, hercynite, margarite, preiswerkite

1. Introduction

The term rodingite was introduced by Bell et al. (1911) for white, calcium-rich rocks hosted by serpentinites in the Dun Mountain ultramafic complex. In general, rodingite is a massive, light-colored rock consisting of Ca- and Ca-Mg-silicates, produced by calcium metasomatism of mafic rock compositions and generally linked to serpentinization of ultramafic rocks (e.g., Coleman, 1977; Frost and Beard 2007; Bach and Klein, 2009; Li et al., 2007). A considerable diversity of rodingites have been documented in ophiolites worldwide (e.g., Schandl, et al., 1989; Tsikouras et al., 2009; Koutsovitis, 2017).

A series of serpentinized and hydrothermally altered Neoproterozoic ophiolites outcrop in the Arabian-Nubian Shield (ANS), specifically in its northwestern most exposure, the Eastern Desert of Egypt (e.g. Boskabadi et al., 2017). One of their major alteration products is rodingite.

Observations of these rodingites offer detailed information on the effects of hydrothermal processes and the physical and chemical conditions of rodingite development provide essential constraints on the tectonic history of their host ophiolites. Yet the rodingites of the ANS have not received much scientific attention, with only a few published studies describing potential rodingite in the Eastern Desert (Takla et al., 1992; Abdel-Karim, 2000; Surour, 2019), and little discussion of the processes involved. In fact, most of the samples described previously as rodingite are altered diabases that, while they bear the characteristic minerals of Ca-metasomatism (hydrogrossular, diopside, prehnite, epidote), also experienced further metasomatism associated with later granitoid intrusions, forming phlogopite and tourmaline, and making their classification as rodingite controversial.

This paper is the first detailed study of rodingite associated with ophiolitic rocks in the Um Rashid area, in the southern part of the central Eastern Desert of Egypt. We present a comprehensive study of the petrological and chemical character of these rodingites, rodingite-related rocks, and the associated serpentinized ultramafic suite. These data support a discussion of the sequence of petrogenetic and metasomatic events that affected this segment of ancient ocean floor; these events may be common to rodingite-bearing ophiolite sequences in the ANS and elsewhere.

2. Geological outline

About 10^5 km^2 of Neoproterozoic rocks outcrop in the Red Sea hills of the Eastern Desert of Egypt and in the southern Sinai Peninsula. Ophiolite sequences are a significant and tectonically important portion of late Neoproterozoic rocks in the central and southern parts of the Eastern Desert of Egypt **(Fig. 1),** but they are absent in the northern part. Ophiolites were

first recognized among the Neoproterozoic basement rocks of the Eastern Desert of Egypt by Garson and Shalaby (1976), but the significance of the Egyptian ophiolites was not appreciated until the study of the Wadi Ghadir ophiolite by El Sharkawy and El Bayoumi (1979). The Egyptian ophiolites are tectonized bodies and mélanges of pillowed metabasalt, gabbro, and variably serpentinized ultramafic rocks. They are all strongly deformed, metamorphosed, and affected by several types of alteration (e.g. Azer and Stern 2007; Gahlan et al., 2015; Gamal El Dien et al., 2019; Abdel-Karim et al., 2020; Ali et al., 2020).

The Um Rashid area, the focus of this study, is located between latitudes 24°55'&25°00'N andlongitudes34°00' &34°10' E. It forms the southern part of the El-Barramiya District and lies on the southern side of the Idfu-Mersa Alam road. The study area is mainly covered by dismembered ophiolites, island-arc assemblages and intrusive rocks **(Fig. 2)**.Ophiolitic rocks are the oldest units in the mapped area and occur in tectonic contact with the volcano-sedimentary island-arc succession **(Fig. 3a)**.

The island-arc assemblages are dominated by metavolcanic rocks and a gabbro-diorite complex; outcrops of metasedimentary rocks are only a few meters in size and not resolvable at the map scale. The metavolcanic sequence makes up a large fraction of the map area. These rocks are mostly massive greyish-green to black in color, with foliation and schistosity apparent in discrete shear zones. Their protoliths extend from mafic to felsic volcanic varieties (metabasalt, meta-andesite, metadacite and metarhyolite) and their pyroclastic equivalents (metatuff and metaconglomerate). Some dykes of variable thickness and composition, both mafic and felsic, cut metavolcanic flow units. The metagabbro-diorite complex is found in a series of small hills in the northeastern part of the map area, and is intruded by granodiorite.

The ophiolitic rocks are dominated by serpentinized peridotites. There are uncommon blocks of metagabbro within the ophiolitic mélange **(Fig. 3b)**, but none large enough to be resolved on the map. Variably altered serpentinites form the main component of the ophiolite sequence. They are mainly found as large masses, usually black or greenish-black. Most serpentinite occurs as massive sheets **(Fig. 3c)**. However, sheared serpentinites are found along shear zones and fault planes **(Fig. 3d)** and serpentinite blocks of various sizes are observed in the ophiolitic mélange. Alteration of the serpentinites is expressed by outcrops of talc-carbonate, magnesite, and listvenite. Magnesite veins are generally concordant to foliation in the sheared serpentinites and rarely pass gradually into a magnesite stockworks. Talc-carbonate rocks are less common and are only observed as sheets and blocks of various sizes within the ophiolitic mélange **(Fig. 3e)**.A few listvenite bodies are developed along shear zones; they form dyke-like bodies or lenses hundreds to thousands of meters long. Listvenite is erosionally resistant, strongly sheared, and pink to red in color due to iron-oxide staining. In some exposures, highly sheared black to grayish-black graphite bearing serpentinites are observed.

Rodingitic rocks appear both in serpentinized ultramafics and in ophiolitic mélange. There is no mention of rodingite in previous literature concerning the Um Rashid ophiolite. They are conspicuous in outcrop because they are white or whitish-grey in colour with black spots, contrasting with the dark-colored ultramafic host rocks. We have observed rodingite-related rock occurring in two distinct modes that we classify as true rodingite and rodingite-like rock.

Rodingite forms blocks and irregular lenses (0.5-1.0 m) in ophiolitic mélange **(Fig. 3f)** at south of G. Um-Rashid. Narrow (5 to 10 cm) blackwall rims of chloritite separate rodingite and serpentinite **(**sketched in **Fig. 3g)**. The chloritite is massive and green; it exhibits a gradual

transition into rodingite. The rodingite and blackwall lenses are commonly tectonized and highly fractured at both macroscopic and microscopic scales.

Rodingite-like rock forms thin light-toned dykes (0.5-1.0 m) with prominent black spots, cutting serpentinized peridotite **(**photograph in **Fig. 3h**, interpretive sketch in **Fig. 3i).**The dykes of rodingite-like rock contain both fully replaced samples and areas with remnants of gabbroic texture and mineral replacement **(Fig. 3j)**, indicating that the protolith was most likely gabbro. A few blocks of gabbro with only minor evidence of rodingitization were also found in the ophiolitic mélange.

3. Analytical methods

Mineral chemical analyses, electron backscatter images, and X-ray mapping were obtained from polished thin and thick sections using a five-spectrometer JEOL JXA-8200 electron microprobe at the Division of Geological and Planetary Sciences (GPS), California Institute of Technology, USA. Surfaces were vacuum-coated with ~15 nm of carbon. Operating conditions were 15 kV, 25 nA, 1 μm beam, 20 s on-peak counting times, and the CITZAF matrix correction routine. The analytical standards used for analyses were synthetic forsterite, fayalite, Mn-olivine, anorthite, TiO_2, and Cr_2O_3; Amelia albite, Asbestos microcline, and Durango apatite.

Selected minerals that could not be definitely identified optically or by electron microprobe were investigated by micro-Raman spectroscopy using a Renishaw InVia instrument. Carbon coats were removed and a 523 nm laser was focused to <1 μm spots on the sample. The spectrometer was calibrated against the 520.5 cm^{-1} main peak of metallic Si. Spectra were collected at Raman shifts from +100 to +4000 cm^{-1} with 10 s integration time. Most phases were

identified by matching peak positions and intensities to the RRUFF library, but serpentine polymorphs were distinguished using the peak assignments of Petriglieri et al. (2015).

Based on the petrographic studies, 25 rock samples (15 serpentinites and 10 rodingitic rocks) were analysed for major, trace and rare earth elements at California Institute of Technology (Caltech, USA) and Activation Laboratories Ltd. (Actlabs, Canada). At Caltech, whole-rock compositions of major and minor elements (Si, Ti, Al, Fe, Mg, Ca, Na, K, P, and Mn as wt. % oxides; Rb, Ba, Sr, Nb, Zr, Hf, Y, Zn, Cu, Ni, Co, Cr, V, La, Ce, Nd, Pb, and Th as elemental μg/g) were determined using a Panalytical Zetium XRF. Sample powders were milled in an agate ball mill, loss on ignition (LOI) determined by weighing before and after firing in air for 1 hour at 1050°C, and fused-glass beads prepared from fired powders by mixing with 9 times their weight in 66.67% $Li_2B_4O_7$-32.83% $LiBO_2$-0.50% LiI flux and fusing at 1200°C. The XRF protocol is calibrated against USGS standards AGV-1, AGV-2, BCR-1, BCR-2, BHVO-2, BIR-1, DNC-1, DTS-2, G-2, GSP-2, MAG-1, NKT-1, NOD-A-1, QLO-1, RGM-2, SBC-1, SCO-1, SDC-1, SGR-1, STM-1, and W-2. USGS standards AGV-2, GSP-2, and RGM-2 are routinely analyzed along with unknowns for quality control and drift correction.

After XRF measurement, 25±1 mg chips of the fused-glass beads are dissolved in new 50 mL polypropylene tubes by refluxing in 2 mL of hot (100°C) 3:1 nitric and hydrofluoric acid for at least 8 hours. After dilution with milli-Q distilled water to 30 mL total volume, elemental concentrations of rare-earth element (REE) and selected major and trace element concentrations (Al, K, Fe, Mn, Cr, V, Ni, Co, Cu, Sc, Sr, Rb, Nb, Ba, Zr, Zn, Cs, Mo, Ta, Hf, Th, W, Pb, and U) were determined with an Agilent Technologies 8800 triple quadrupole ICP-MS. A working curve for instrument sensitivity was developed using a blank fused bead from the same batch of

flux along with USGS standards AGV-2 and RGM-2. To control for quality, additional USGS standards (DTS-2, BCR-1, G-2) were included as unknowns.

In the Actlabs (Canada) analyses, the major oxides were measured by lithium metaborate/tetraborate fusion ICP-AES. Trace and rare earth elements were measured by ICP-MS following lithium borate fusion and acid digestion. Loss on ignition (LOI) is determined by weight difference after ignition at 1000ºC. Precision and accuracy were controlled by analysis of international reference materials and replicate analyses and are 1% for major elements and 2% to 5% for trace elements. Full details are on the laboratory website (actlabs.com).

4. Petrography

Petrographic studies were carried out on both thin and polished sections of the rodingites and their host serpentinite. Modal abundances were estimated by optical microscopy, with key mineral identifications verified where necessary by electron microprobe and Raman spectroscopy.

4.1. Serpentinites

Ultramafic samples are variably serpentinized and include both massive and sheared varieties. Massive serpentinite consists essentially of serpentine minerals with minor carbonates, amphiboles, opaques, and brucite. Despite the high degree of serpentinization, rare fresh relics of primary olivine, pyroxene and chromian spinel are observed. The original textures of the ultramafic rocks have been almost completely obliterated, but the geometric configurations of the original mafic minerals help to determine their protoliths. The abundance of bastite after orthopyroxene **(Fig. 4a)** and mesh texture after olivine **(Fig. 4b)** indicates harzburgite and dunite

protoliths. Fresh olivine relics in most samples are strained crystals with kink bands, characteristic of deformed mantle tectonites from ophiolites. In one serpentinite collected near the granodiorite intrusion, there are also unstrained relict olivine crystals. Chromian spinel, magnetite and sulfides are the main opaque minerals. Deep reddish-brown chromian spinel occurs as subhedral to euhedral disseminated crystals and as irregular grains. Along grain boundaries and cracks, chromian spinel is partly replaced by inner rims of ferritchromite and outer rims of Cr-magnetite **(Fig. 4c)**.Brucite appears as platy or fibrous crystals intermixed with serpentine minerals and as veinlets. Very few sulfide grains are present; they may be pyrite, arsenopyrite, or chalcopyrite.

Partly serpentinized peridotite has similar textures and compositions to the massive serpentinite, but with higher proportion of fresh minerals (up to 30 vol. %). The fresh relics of primary olivine form anhedral, strained, and cracked crystals dissected by networks of serpentine veins **(Fig. 4d)**. Subhedral fresh orthopyroxene (enstatite) and clinopyroxene (diopside) crystals are both present. The clinopyroxene displays metamorphic foliation and lineation **(Fig. 4e)**, typical of mantle samples that have experienced high-temperature subsolidus plastic deformation.

Sheared serpentinite is similar in mineralogy to massive serpentinites, but is brecciated and expresses a clear schistosity defined by subparallel alignment of serpentine flakes **(Fig. 4f)**. Some samples of sheared serpentinite are rich in carbonates (10-25 vol. %) and some contain occasional fibrous crystals of tremolite–actinolite. Fractures in sheared serpentinite are filled with chrysotile, quartz and carbonate minerals. No relics of fresh olivine orpyroxenes are found in the sheared serpentinites; chromian spinel is the only surviving primary mineral.

4.2. Rodingitic rocks

Based on field relations and mineral assemblages, we divide the rodingitic rocks into two types: typical rodingite and rodingite-like rock. Some samples of rodingite-like rock are completely replaced whereas others preserve primary textures from their gabbro protoliths.

Typical rodingite is medium- to coarse-grained with whitish colour and black spots. It consists essentially of calcium-rich minerals including garnet, pyroxene, vesuvianite, and chlorite, plus minor prehnite and opaque minerals. Garnet occurs as dissected crystals (0.5 to 3 mm in diameter), spotted with very fine specks of vesuvianite and scarce inclusions of diopside and transformed along the margins into chlorite **(Fig. 5a)**. Clinopyroxene occurs as coarse anhedral crystals of diopside **(Fig. 5b, c)**, partly replaced along the margins and cleavage planes by chlorite, garnet and secondary diopside and amphibole. Rarely, secondary diopside forms fibrous or acicular crystals around or within vesuvianite aggregates. Vesuvianite, in addition to the fine inclusions in garnet, is also found as subhedral to anhedral, medium to coarse crystals **(Fig. 5c, d)**. Chlorite occurs as interstitial crystals and along cleavage planes in clinopyroxene and cracks in garnet (Fig. 5a, b, c, d). Prehnite occurs as wormy veinlets and in the cores of highly altered plagioclase crystals.

The chloritite found as narrow blackwall rims around outcrops of rodingite is a nearly monomineralic, dark green rock. In addition to the dominant chlorite phase, there are minor amounts of rutile, epidote, corundum and opaque minerals. Scarce relics of serpentine can be found in the chloritite. Chlorite appears as fine dense flaky aggregates with perfect foliation. It is pale green and faintly pleochroic in plane polarized light; under crossed nicols it shows an anomalous brown interference color. Rutile is present as fine anhedral red crystals or as tabular red crystals **(Fig. 5e)**. Corundum occurs as aggregates of subhedral to anhedral crystals **(Fig. 5f)**.

Rodingite-like rock is fine- to medium grained and white with black spots. Aluminum-rich minerals are the main constituent of rodingite-like rock. They include corundum, hercynite, micas and plagioclase as well as minor secondary amphibole, clinozoisite, prehnite, diaspore and epidote. Although the rodingite-like rock is the product of extensive alteration and replacement, gabbroic textures and relics of primary minerals characteristic of gabbro are preserved in some samples. The rodingite-like rock samples are further divided into partly and fully rodingitized groups based on the modal abundance of preserved primary minerals and textures. The alteration assemblage is the same in these two groups. Corundum occurs as colorless, subhedral to euhedral crystals (**Fig. 6a**). Hercynite, a green spinel-group mineral, occurs as subhedral to anhedral porphyroblasts and as fine aggregates (**Fig. 6 a, b)**. The fine hercynite aggregates are only found in association with amphibole and chlorite in areas of coronitic texture. Mica-group minerals include preiswerkite, margarite and muscovite; all take the form of acicular or tabular crystals (**Fig. 6c**). Plagioclase occurs as fine to medium-sized subhedral crystals. The primary calcic plagioclase is almost completely albitized, but rare relics of labradorite are recorded and albite twinning of the primary plagioclase can still be recognized **(Fig. 6d)**. Clinozoisite and prehnite replace plagioclase and occur as fine crystals and fine columnar aggregates, respectively. Epidote also occurs as veinlets and as small anhedral crystals rimming green spinel. Diaspore, an aluminum hydroxide mineral, occurs as anhedral (**Fig. 6c**) or acicular crystals. Secondary amphibole is represented by fibers or clusters of acicular green actinolite crystals. Chlorite occurs as fine aggregates.

5. Mineral Chemistry

The electron microprobe was used in this study for two purposes: to identify those essential and accessory minerals that could not be fully determined by optical petrography, and to quantitatively analyze those minerals that have significant solid solution ranges and occur as homogeneous grains large enough for single-phase analysis. Not all the minerals mentioned above were suitable for quantitative microprobe analysis. This section summarizes mineral chemistry results, grouped by rock type and then by mineral phase.

5.1. Serpentinite

Both silicate and non-silicate minerals were analyzed in serpentinite samples. The analyzed silicate minerals include olivine, pyroxene, amphibole, serpentine and chlorite; non-silicate minerals include chromian spinel, magnetite and brucite. The mineral chemistry dataset for serpentinite, including calculated structural formulae, is given in the Electronic Appendix (Supplementary Tables 1S-8S).

5.1.1. Olivine

Most of the analyzed olivine relics are unzoned, except for sample 53, which exhibits a relatively wide compositional range, from Fo (molar $Mg/[Mg+Fe_T]$) 0.75 to 0.96. The unzoned olivine crystals have homogeneous and high Fo contents (91-92) in the common range of primary mantle olivines (e.g. Pearce et al., 2000; Takahashi et al., 1987). NiO contents in the unzoned olivines range between 0.20 and 0.31 wt.% (average 0.25 wt.%), notably lower than is typical of mantle olivines (Takahashi et al., 1987). The wide range in the Fo content in sample 53 can be attributed to recrystallization of olivine during a thermal metamorphic event linked to the intrusion of granodiorite (see discussion, section 7.2).

5.1.2. Pyroxenes

A few fresh relics of orthopyroxene were analyzed in serpentinized peridotite; it is identified as enstatite**(Fig. 7a)**(nomenclature of Morimoto et al.,1988).Orthopyroxene has high Mg# (molar Mg/[Mg+Fe_t) ~ 0.92) and low TiO_2 (<0.02 wt. %), Al_2O_3 (1.35-1.84 wt. %), CaO (0.95-1.31wt. %),and Cr_2O_3 (0.62-0.81 wt. %) contents. The Mg# of orthopyroxene is very similar to that of olivine (0.91-0.92), suggesting that these two phases equilibrated under high-temperature mantle conditions (Uysal et al., 2016). The low$Al_2O_3$and CaO contents are similar to those of primary mantle orthopyroxenes (Ishimaru et al., 2007). One pseudomorph after enstatite includes both lamellae of fresh orthopyroxene and zones of fibrous, poorly crystalline clinopyroxene-rich material (see Fig. 4e). Its chemical composition at electron probe scale is subcalcic (0.61-0.83, average 0.73 apfu), nearly Fe-free (Mg# ~0.99), cannot be mapped precisely into pyroxene components, and shows low totals. Its Raman spectrum shows weak diopside peaks as well as a large OH-absorption. This material is not relict igneous clinopyroxene; it is an alteration product indicating incipient Ca-metasomatism of the serpentinite.

5.1.3. Chromian spinel

Chromian spinels relics have homogeneous fresh cores of Cr-spinel surrounded by inner rims altered to ferritchromite and outer rims of Cr-magnetite. In most crystals, Cr_2O_3, Al_2O_3 and MgO show a systematic decrease from core to rim, whereas FeO_T increases outwards. This sequence is commonly recognized in spinels altered under hydrothermal conditions (Barnes,

2000). The fresh cores show Cr# (molar Cr/[Cr+Al)) between 0.64 and 0.67 (average 0.66) and Mg# between 0.45 and0.58 (average 0.54).

5.1.4. Tremolite

Structural formulae of amphibole were calculated on the basis of 23 oxygen atoms in the anhydrous total using the 13-CNK method of Leake et al. (1997); they are calcic amphibole, exclusively tremolite. The low TiO_2 (<0.1 wt. %) content of amphibole and the discrimination diagram proposed by Keeditse et al. (2016) for separating magmatic and post-magmatic amphibole both indicate that it is secondary (Girardeau and Mevel, 1982), formed by alteration of primary olivine and pyroxene **(Fig. 7b)**.

5.1.5. Serpentine minerals

Serpentine is divided petrographically into matrix and vein-type. Matrix serpentine is chemically homogeneous and near ideal antigorite stoichiometry (i.e., (Mg+Fe)/Si is consistently less than 1.5, averaging 1.41). Several spots of matrix serpentine were checked by Raman spectroscopy and verified to be antigorite by the criteria of Petriglieri et al. (2015). Vein-forming serpentine has lower $Mg^{\#}$ (0.86-0.92) than matrix serpentine (0.88-0.99) and often approaches ideal chrysotile stoichiometry (i.e. (Mg+Fe)/Si ~ 1.5); Raman spectra confirms that the veins are chrysotile. Vein and matrix serpentine both show low concentrations of TiO_2 ($\leq$ 0.02 wt. %.). Our petrographic studies indicate that serpentinite sample M9 had a dunite protolith; serpentine in this sample is richer in Cr_2O_3 and NiO than in the samples of harzburgite parentage.

Sample M9 contains occasional ~100 μm phyllosilicate grains whose analyses at electron probe scale are very rich in both Ni and Fe and very low in Al. Detailed high-magnification

examination with a field-emission scanning electron microscope shows that these domains are not a single phase. They are fine-grained (100 nm-scale) porous aggregates of a Ni-rich serpentine (likely pecoraite or népouite) and a Fe-rich serpentine (likely greenalite or cronstedtite). Given the very small grain-size, further characterization is difficult and would require further study beyond the scope of this work.

5.1.6. Chlorite

The chlorite in sample 53 shows limited chemical variation in SiO_2, MgO and Cr_2O_3. This chlorite is mainly classified (Hey, 1954)as penninite with minor talc-chlorite**(Fig. 7c)**. The chemical composition of chlorite can be used to determine the temperature of its formation (e.g. Kranidiotis and MacLean 1987; Cathelineau and Nieva 1985). The temperatures for disseminated chlorite formation, calculated with the geothermometry calibration of Kranidiotis and MacLean (1987), range between 124 and 181°C, with an average of 162°C.

5.1.7. Magnetite

In the disseminated magnetite analyses, total Fe as FeO is the main oxide (88.29-91.99 wt.%),with negligible amounts of MnO, Cr_2O_3 and NiO. Oxides such as SiO_2, CaO, Na_2O, K_2O and P_2O_5that appear in the analyses probably represent beam overlap with or secondary fluorescence from adjacent phases. The disseminated magnetite plainly differs from the Cr-magnetite that rims chromian spinel; the latter is much richer in Cr_2O_3.

5.1.8. Brucite

Brucite is a magnesium hydroxide mineral, nominally $Mg(OH)_2$. Hypothetical pure brucite would contain 71.09 wt. % MgO and show an analytical total of 71.09 wt. %. In fact, MgO is the main oxide (71.64-79.57 wt. %), with smaller amounts of SiO_2 (0.93-9.75 wt. %) and FeO (2.53-4.90 wt. %); analytical totals range from 80 to 89 wt. %. Other oxides (Al_2O_3, MnO, Cr_2O_3 and CaO) occur in minor amounts. It is unclear whether the brucite contains chlorite layers as defects or whether the electron probe beam tended to overlap adjacent serpentine, given the very small grain size of brucite patches.

5.2. Rodingitic rocks

Microprobe analyses and calculated structural formulae of minerals in rodingite and rodingite-like rock are presented in Supplementary Tables 9S-22S. Analyzed minerals in the rodingite samples include garnet, pyroxene, vesuvianite, chlorite and ilmenite, while those in the rodingite-like rock samples include hercynite, corundum, diaspore, plagioclase, micas, amphiboles, clinozoisite, and prehnite.

5.2.1. Garnet

Garnet analyses cluster at the Al-rich and Fe-rich ends of the grossular-andradite solid-solution series. The electron microprobe does not directly measure water in the garnet structure, but low analytical totals on well-polished garnets indicate the presence of a significant hydrogarnet component in many cases. This is supported by energy-dispersive X-ray spectra that demonstrate the absence of any unanalyzed elements heavier than C and by Raman spectra with very strong OH vibration bands. Although there are multiple possible substitution mechanisms

for minor hydrogen in garnet, the component that can host the largest amount of water is katoite, $Ca_3Al_2(OH)_{12}$, and we include this molecule in our garnet end-member fractions.

Grossular is composed mainly of SiO_2 (38.4-39.8 wt.%) and CaO (35.5- 37.2 wt.%), with variableAl_2O_3 (13.9-21.8 wt.%) and FeO_t (1.0-8.3 wt.%). The increased abundance of FeO_t in andradite (9.27-23.82 wt.%) is compensated by lower weight fraction of SiO_2 (32.2-36.8 wt.%), CaO (31.5-35.3 wt.%) and especially Al_2O_3 (3.0-9.3 wt.%). Entirely aside from the issue of hydration, andradite shows a lower apparent analytical total than grossular because the Fe in this mineral is dominantly Fe_2O_3, whereas the electron probe totals assume total Fe as FeO; for garnets with up 23 wt.% FeO_t, this accounts for up to 2.3 wt.% deficit in the total.

After correcting for Fe_2O_3, the analytical total deficits of both andradite and grossular are correlated with deficits in Si relative to 3 atoms per formula unit (apfu), which is consistent with H_2O being incorporated by the hydrogarnet substitution. We find hydrous grossular with up to 6 mol.% katoite component or 1.5 wt.% H_2O and hydrous andradite with up to 12.3 mol.% katoite or 2.7 wt.% H_2O. The abundance of hydrated garnets with substantial Si deficits in rodingite suggests a component of desilicification associated with their formation. Hydrogrossular may be formed after diopside (Frost and Beard, 2007) but the more common reaction pathway is decomposition of anorthitic plagioclase to zoisite or prehnite followed by alteration to hydrous garnet (Schandl et al., 1989).

5.2.2. Clinopyroxene

Petrographic studies indicate that most of the clinopyroxene in rodingite is secondary, although a few primary relics are present. The major oxides in clinopyroxene are SiO_2 (50.0-55.3 wt.%), CaO (23.0-25.8 wt.%), MgO (13.7-17.7 wt.%) and FeO_t (2.8-8.1 wt.%). Primary

clinopyroxene relics are richer in MgO (15.8-17.7 wt.%) and lower in FeO_t(2.8-3.3 wt.%), with higher Mg# (0.90-0.92)than the more common secondary clinopyroxene (14.5-16.4 wt.% MgO; 3.2-6.2 wt.% FeO_t; Mg# 0.75-0.89). On the pyroxene nomenclature diagram(Morimoto et al.,1988), all the clinopyroxene analyses are diopside**(Fig. 7a)**. The compositions of the fresh clinopyroxene relics are typical of clinopyroxene in ophiolitic gabbro (Mogahed and Saad, 2020).

5.2.3. Vesuvianite

The essential oxides in vesuvianite areSiO_2(36.3-38.2 wt.%), CaO (32.2-37.0 wt.%) and Al_2O_3(16.3-21.6 wt.%), with subordinate FeO_t(1.1-6.6 wt.%) and MgO (0.0-3.7 wt.%). Some vesuvianite analyses have low analytical totals and low birefringence, suggesting incorporation of an unanalyzed volatile component(Hatzipanagiotou and Tsikouras, 2001).

5.2.4. Chlorite

There is a wide range of chlorite compositions both within and between samples, presumably the result of a combination of multiple ferromagnesian parent minerals (amphibole, pyroxene and biotite) and evolving conditions of pressure, temperature, and water activity. Major oxide variations are dominated by SiO_2 (21.7-30.1 wt.%), MgO (9.9-27.8 wt.%), Al_2O_3(14.2-24.8wt.%), and FeO_t (9.1- 33.0 wt.%). TiO_2, Cr_2O_3, K_2O and Na_2O are all negligible. A few spots of chlorite have significant concentrations of CaO (up to 3.8 wt.%), attributable to incorporation of interlayer smectite.

According to the classification scheme of Hey (1954), chlorite is mainly pycnochlorite and ripidolite with minor clinochlore and some outliers in other named fields **(Fig. 7c)**.The

calibrated geothermometer equation of Kranidiotis and MacLean (1987)yields chlorite formation temperatures in rodingite between 217°Cand 375°C.

5.2.5. Ilmenite

Ilmenite is composed mainly of TiO_2(42.2- 51.3 wt.%)and FeO_t(44.3-52.8, wt.%), with measurable but minor MnO (1.5-2.6 wt.%).

5.2.6. Hercynite

Analyses of hercynite have been filtered to remove points with SiO2 > 0.5 wt.%, likely due to contamination from neighboring phases. Analytical totals of hercynite in sample R41 are low (93-98 wt.%), probably due to rounding of small grains during polishing, but structural formulae show valid spinel stoichiometry. Hercynite consists mainly of Al_2O_3andFeO_t, with minor MgO (2.4-3.6 wt.%). Cr_2O_3 is below detection. On the Cr^{+3}-Fe^{+3}-Al^{+3}ternary classification diagram of spinel, these analyses are nearly perfect end-member hercynite and plot entirely in the hercynite field **(Fig. 7d)**. This spinel-group material is clearly distinct from primary igneous chromite.

5.2.7. Corundum and diaspore

The Al-rich minerals include corundum and diaspore. Corundum is essentially pure Al_2O_3 with high totals and up to 0.4 wt.% FeO_t. Diaspore has up to 1 wt.% FeO_t (goethite component) and is distinguished by low analytical totals (87.2-94.0 wt.%) reflecting the presence of structural OH.

5.2.7. Plagioclase

Apparent plagioclase compositions vary significantly from albite through oligoclase and andesine to labradorite. The plagioclase is all strongly altered and mottled with replacement phases that make it challenging to obtain quality electron probe analyses with 100% totals and no contamination. Only two spots yielded candidate primary labradorite compositions that would be reasonable igneous minerals in a gabbroic protolith. The other, more sodic, plagioclase spots are likely to be secondary plagioclase developed during alteration and metamorphism.

5.2.8. Mica

The analyzed mica-group minerals are represented by margarite, preiswerkite, and minor muscovite. Preiswerkite, nominally $NaMg_2Al(Al_2Si_2)O_{10}(OH)_2$(Keusen and Peters, 1980), is a rare sodic trioctahedral mica. In our samples there is major replacement of Mg by Fe, but in all analyses Mg > Fe and so the name preiswerkite is appropriate. Margarite, nominally $CaAl_2(Al_2Si_2)O_{10}(OH)_2$, has in our samples substantial substitution of Na (up to 0.57 apfu, but more commonly ~0.32 apfu), charge-compensated by partial trioctahedral occupancy by Fe and Mg. Muscovite deviates from ideal $KAl_2(AlSi_3)O_{10}(OH)_2$ due to vacancies on the K site variably charge-compensated by anomalies in the tetrahedral Al/Si ratio or by partial trioctahedral occupancy by Al or Mg.

5.2.9. Amphibole

Amphibole in rodingite-like rock exhibits a substantial compositional range. In the classification scheme of Leake et al.(1997),all points are calcic amphibole and variously classify

as ferro-pargasite orferro-tschermakite, with one point each of pargasite and magnesio-sadanagaite. With <0.1 apfu of Ti, they are of secondary origin(Girardeau and Mevel, 1982).

5.2.10.Clinozoisite

A handful of clinozoisite crystals were noted in one rodingite-like rock sample; it is very close to nominal end-member $Ca_2Al_3(Si_2O_7)(SiO_4)O(OH)$ composition, with only small amounts of Fe_2O_3 (≤0.76 wt.%) or Na_2O (≤0.41 wt.%)observed in a couple spots. Clinozoisite is a common epidote group mineral that represents an alteration product of plagioclase; primary Ca-bearing plagioclase typically breaks down to albite and Ca-rich clinozoisite or prehnite.

5.2.11. Prehnite

Prehnite, like clinozoisite, forms during alteration of primary Ca-bearing plagioclase to albite and acts as a sink for Ca. Prehnite was found and analyzed in one rodingite-like rock sample; it is essentially stoichiometric $Ca_2Al_2Si_3O_{10}(OH)_2$with negligible concentrations of all other oxides.

6. Geochemistry

6.1. Serpentinites

Fifteen representative serpentinite samples were analyzed for whole rock geochemistry and the results are given in Tables 1 and 2. All the serpentinite samples have high LOI values, between 11.2 and 15.4 wt.%. The highest value of LOI is recorded in the carbonate-rich sheared sample (59).

The modal percentages of primary minerals cannot be accurately determined due to extensive serpentinization. Neglecting changes in composition due to alteration, we applied a classification based on normative composition (Table 1), which classifies the samples mainly as harzburgite with minor dunite **(Fig.8a)**, in agreement with petrographic assessments. Two samples are shifted into the lherzolite field by enrichment in CaO hosted by secondary carbonates.

The serpentinite samples assigned to dunite protoliths (>80 wt.% normative olivine) have lower silica contents (36.7-37.0 wt.%) and higher MgO (41.6-42.4 wt.%) than those formed from harzburgite (37.0-41.8 wt.% SiO_2 and 37.0-39.4 wt.% MgO). No significant variations were noted in other major oxides. All the analyzed samples are very low in CaO (< 1.0 wt. % except for carbonate-bearing samples) and Al_2O_3 (<1.0 wt. %), consistent with the low modal clinopyroxene abundance and absence of plagioclase. The serpentinites have high whole-rock Mg# with limited variation(0.90-0.92, av.0.91),typical of oceanic peridotites (Bonatti and Michael, 1989) and similar to the Mg# of other serpentinites in the ANS (e.g., Gahlan et al., 2020; Ali et al., 2020; Abdel-Karim et al., 2020).

Trace element contents among the analyzed serpentinite samples vary by a factor of 3 to 10 for most well-resolved elements (Table 2). They are depleted in most trace elements but they are enriched in compatible elements (Cr, Ni and Co) and above primitive mantle in selected fluid-mobile elements (Li, As, Sb, Pb, Sr, Cs and U).

On primitive mantle (PM) normalized trace element patterns (normalization values of McDonough and Sun, 1995) (**Fig. 8b**), the depletion of most trace elements in serpentinite samples is evident. Positive anomalies in Cs, Pb and U are prominent. Enrichment of these elements in serpentinites has been judged in various cases to have been present in the protolith

(Godard et al., 2008) or to have been added from fluids(e.g., seawater) during serpentinization (Deschamps et al., 2013). Serpentinites contain suitable hosts for sequestering and concentrating each of these elements from migrating fluids: As and Sb can be hosted in both serpentine phases and sulfide minerals; carbonates are known to host U, Sr and Pb. Scambelluri et al. (2019) noted that enrichment in As and Pb are characteristic of fore-arc serpentinites in particular.

The concentrations of REE of serpentinites are given in Table 3 and their chondrite-normalized REE patterns (normalization values of Evensen et al., 1978) are plotted in **Fig.8c**. The REE abundances vary markedly among the serpentinite samples, by an order of magnitude in LREE and a factor of 4 in HREE. Most samples show a modest enrichment in LREE [$(La/Lu)_N$= 1.26-4.30] with nearly flat HREE [$Gd/Lu)_N$ = 0.97-1.38]. Although fresh mantle harzburgites and dunites are characterized by strong to extreme LREE depletion, serpentinites often show LREE enrichment, presumably as a result of transfer from serpentinizing fluids (Deschamps et al., 2013). Among the serpentinite samples, there is no evident correlation between trace and major elements or between trace elements and primary mineral modes. In particular, the dunites are in the middle range of samples for nearly all analyzed elements. This is consistent with the trace element signature being dominated by enrichment during serpentinization rather than by primary source or melting phenomena.

The serpentinite samples have widely variable negative or positive Eu anomalies [Eu/Eu* = 0.45-2.51], despite neither containing nor having interacted with plagioclase. The Eu budget of these samples is also likely derived from serpentinizing fluids (Paulik et al., 2006). In this case, positive Eu anomalies likely result from substitution of $Eu^{2+}$for Ca^{2+} in carbonates (either at the source of the CO_2-bearing fluids or locally in the samples) (Boedo et al., 2015).On the other

hand, negative Eu anomalies reflect the occasional presence of talc, a phase that is known to exclude Eu relative to neighboring REE (Cardenas-Párraga et al., 2017).

6.2. Rodingitic rocks

Major and trace element contents of 10 rodingitic samples(4 rodingite and 6 rodingite-like rocks)are given in Tables4 and 5. The division of the rodingitic samples into categories on the basis of mineralogy is reflected in well-defined groups of distinctive whole-rock chemistry, most notably in concentrations of SiO_2, Al_2O_3, MgO, Fe_2O_{3t}, and CaO and LOI. Typical rodingite samples are richer in CaO (20.6-23.9 wt.%), Fe_2O_{3t} (6.9-20.7wt.%), and MgO (8.4-13.6wt.%) compared to rodingite-like rocks (5.9-13.4wt.% CaO, 1.9-4.8 wt.% Fe_2O_{3t}, 2.1-10.6wt.% MgO). On the other hand, typical rodingite is lower in SiO_2 (33.2-39.1 wt.%), Al_2O_3 (9.3-14.8 wt.%), and K_2O (≤0.03 wt.%) than the rodingite-like rocks (35.3-45.1 wt.%SiO_2 , 28.0-32.6wt.%Al_2O_3, 0.8-1.8 wt.% and K_2O).

The high concentration of CaO in typical rodingite reflects the abundance of calcium–rich minerals including as garnet, diopside and vesuvianite. Elevation in MgO reflects the formation of secondary Mg bearing minerals including chlorite and diopside. Elevated values of LOI in the rodingite reflect the presence of hydrous minerals including chlorite, vesuvianite, and hydrogarnet.Al_2O_3/CaO ratios in typical rodingite are low (0.45-0.65 by weight) and they lack normative corundum. Rodingite-like rock samples, by contrast, are highly enriched in Al_2O_3, hosted in the highly aluminous phases corundum, diaspore, preiswerkite, margarite, hercynite, and plagioclase. They have notably high Al_2O_3/CaO(1.8-5.6) and normative corundum (3.2-13.0wt.%). Plotting all the rodingite and rodingite-like samples on an A-C-F diagram **(Fig. 9a)** shows that the rodingite samples lie near the field of rodingite defined by Coleman (1977),

although one sample contains an unusually high concentration of Fe_2O_{3t}.The samples of rodingite-like rock plot near the A apex due to aforementioned enrichment in Al_2O_3 and abundance of Al_2O_3–rich minerals.

The trace element contents of the rodingitic rocks separate into well-defined groups of rodingite, partly rodingitized rodingite-like rock, and highly rodingitized rodingite-like rock (Table 5). If all the rodingites are derived from similar gabbroic protoliths, then these variations testify to major metasomatic redistribution of elements during rodingitization. However, their initial concentrations and differential mobility during alteration may also reflect significant differences between their source lithologies. Most rodingite-like samples, especially the highly rodingitized ones, have higher concentrations of all incompatible trace elements except Nb and Ta (and, in one sample, Th) than do the typical rodingites. The partly rodingitized rodingite-like rocks are mostly intermediate in trace element enrichment between the other two groups. Rodingite samples, by contrast, are richer in compatible elements (Cr, Ni, Co and V)than rodingite-like rocks. One of the most striking features of the rodingite-like rock is its abnormal enrichment in Sr (up to 3438 μg/g) and Zr (up to 1181 μg/g).These values are notably higher than those in the less-altered mafic suite of the associated ophiolite (gabbro). These features will be discussed in detail below (section 7).

The PM-normalized trace elements patterns of the rodingitic rocks are shown in **Fig.9b**. The typical rodingites have surprisingly flat trace element patterns, with all elements (except Cs, Rb, and Sr) plotting within a small range around 2× PM. By contrast, the highly rodingitized rodingite-like rocks have dramatic enrichments and anomalies, being over 100× PM in concentrations of most incompatible elements, including both large ion lithophile elements (K, Rb, Sr, Ba, U, Th)and the high field strength elements Zr and Hf. However, they are strongly

depleted (anomalies of 2-3 orders of magnitude) in the HFSE Nb and Ta. The partly rodingitized samples share some of these features, with about one order of magnitude lower LILE but similar patterns of anomalies.

REE concentrations in the rodingitic samples are given in Table 6 and chondrite-normalized REE patterns are plotted in **Fig. 9c**. The distinctions among the rodingite, partly rodingitized, and highly rodingitized rodingite-like samples are obvious in their REE patterns. As with the extended trace elements, truerodingite samples show low concentrations (ΣREE = 9-13 μg/g, av. 11 μg/g) and very limited range of variation. Their REE patterns are nearly flat, gently depleted in LREE with slight positive Ce anomalies that may reflect oxidizing conditions during alteration that stabilized some Ce^{4+}. The samples of rodingite-like rock are highly variable in REE concentration, ΣREE from 15-595 μg/g, with light to moderate enrichment in LREE [$(La/Lu)_n$=3.1-21.3]. The partly rodingitized samples of rodingite-like rock, preserving primary gabbroic minerals and textures, are systematically lower in REE than the fully replaced rodingite-like rocks and display in two cases significant positive Eu anomalies (Eu/Eu*=1.42 and 4.13).

7. Discussion

7.1. Protolith and geodynamic setting of serpentinites

Based on petrographic observation and geochemical data, the protoliths of Um Rashid serpentinites are strongly depleted mantle harzburgites and dunites. Their Mg#, Ni, and Cr contents and low Al_2O_3, CaO, and incompatible trace elements are all characteristic of highly refractory mantle peridotites, residual to high degrees of melt extraction (Bonatti and Michael, 1989; Parkinson and Pearce, 1998; Deschamps et al., 2013). Specifically, with the exception of

carbonate-hosted CaO in some samples, the very low Al_2O_3 and CaO of these serpentinites are most similar to fore-arc peridotites **(Fig. 10a)**. On an MgO/SiO_2 vs. Al_2O_3/SiO_2 diagram (Jagoutz et al., 1979; Hart and Zindler, 1986), the Um Rashid serpentinite plots at low Al_2O_3/SiO_2($\leq$0.03)**(Fig. 10b)**, overlapping the fore-arc field (Deschamps et al., 2013) and the most depleted end of the abyssal peridotite field. The serpentinite samples with dunite protoliths plot above the terrestrial mantle array, suggesting that a process other than progressive fractional melt extraction was responsible for increasing their olivine/orthopyroxene ratios (Deschamps et al., 2013).

Even in almost completely serpentinized peridotites, the chemistry of relict primary minerals offers a tool to infer the tectonic environment of their protoliths (e.g., Dick and Bullen, 1984; Barnes and Roeder, 2001; Ohara et al., 2002; Arif and Jan, 2006). Fo content of fresh olivine, like Mg# of whole rocks, increases with melt depletion and is less sensitive to modification during serpentinization. Chromian spinel is notably sensitive to changes in variables such as temperature, pressure, oxygen fugacity, bulk rock composition, and fluid composition (e.g. Dick and Bullen, 1984; Barnes and Roeder, 2001; Arif and Jan, 2006; Gamal El Dien et al., 2019) that in turn indicate particular tectonic settings and petrogenetic processes. Spinel in mid-ocean ridge and back-arc basin peridotites generally has Cr#<50, whereas spinel in fore-arc harzburgites generally has higher Cr# (60-80) and spinel in boninite lavas typically has even higher Cr# (70-90) (Barnes and Roeder 2001; Ohara et al., 2002).

In the Um Rashid case, the low TiO_2 (<0.02 wt. %) and high Cr# (0.64-0.67) of relict primary chromian spinel in serpentinite point, like the whole-rock indicators, to strongly depleted mantle residues after extensive partial melt extraction. Such high extents of melt extraction are most common in supra-subduction zone setting, specifically in the fore-arc (e.g. Dick and

Bullen, 1984; Ishii et al., 1992; Bloomer et al., 1995). On the Cr# versus Mg# discrimination diagram, the fresh chromian spinel relics plot in the region of fore-arc peridotite **(Fig. 11a)**, at estimated degrees of partial melting from 35–38% **(**Parkinson and Pearce, 1998; Pearce et al., 2000).Although high Cr# spinel can also form by extensive melt–rock interaction (e.g. Parkinson and Pearce, 1998; Pearce et al., 2000), low TiO_2 contents are not consistent with the products of melt-rock reaction, which tend to be Ti-rich. Spinel in Um Rashid serpentinite resembles many other examples in ANS ophiolites assigned by numerous authors to fore-arc settings (Azer, 2014; Gahlan et al., 2015; Boskabadi et al., 2017; Abdel-Karim et al., 2020; Ali et al., 2020; Gahlan et al., 2020).

Pyroxene relics can provide further insight into peridotite petrogenesis (e.g., Pagé et al., 2008; Xiong et al., 2018). The high Mg#, low Al_2O_3 content, and low $Cr_2O_3$of relict orthopyroxene are all consistent with orthopyroxene from known fore-arc peridotites (Pagé et al., 2008; Xiong et al., 2018) and outside the field of abyssal peridotites **(Fig. 11b, c).**The composition of orthopyroxene in the current suite is consistent with that of other serpentinites of the ANS assigned to fore-arc settings (e.g., Abdel-Karim et al., 2020; Gahlan et al., 2020).

Olivines becoming increasingly magnesian with progressive melt extraction. To the extent that different extent of melting are characteristic of tectonic setting (e.g., supra-subduction zone vs. mid-ocean ridge), olivine too is helpful for distinguishing the setting of serpentinite protoliths (Parkinson and Pearce, 1998). Mg-rich olivine ($Fo_{0.91-0.92}$) in the Um Rashid samples again points to the high extents of melt extraction most commonly recorded by fore-arc peridotites. Similar high-Fo olivine have likewise supported assignment of numerous other ANS ophiolite mantle sections to fore-arc settings (Khalil and Azer, 2007; Stern et al., 2004; Gahlan et al., 2020).

In short, all the mineralogical and whole-rock evidence points to emplacement of the mantle section of the Um Rashid ophiolite, like other ANS ophiolites, as fragments of oceanic lithosphere above the fore-arc of a subduction (e.g. Azer and Stern, 2007; Gahlan et al., 2020).A number of tectonic and petrogenetic models have been proposed to explain formation and obduction of fore-arc peridotites in Egypt (e.g. Azer and Stern, 2007; Ali et al., 2020; Abdel-Karim et al., 2020); the most recent such model (Abdel-Karim et al., 2020) is summarized in **Fig. 12**. Opening of the Mozambique Ocean between East and West Gondwana is followed by development of an incipient arc stage and then by full development of a mature arc system with high slab-derived fluid flux and large degrees of melting in the fore-arc mantle.

7.2. Formation of metamorphic olivine in serpentinite

Upon prograde metamorphism, serpentine can dehydrate and produce metamorphic olivine (e.g., Nozaka, 2003; Evans, 2010). Such metamorphic olivine typically lacks chemical zonation or evidence of ductile deformation (e.g., undulatory extinction; Khalil and Azer, 2007; Evans, 2010). According to Evans (2010), metamorphic olivine with low Fo content can form by breakdown of Fe-rich serpentine, itself a product of relatively high-temperature serpentinization.

Olivine crystals in sample 53 have unusual compositions, with a wide range of Fo content (0.79 to 0.96). These are quite different from the homogeneous Fo_{91-92} in residual peridotites. Petrographically, sample 53 contains both strained olivine with kink bands and unstrained olivine. Olivine with similar characteristics has been reported in serpentinized peridotites from other ANS ophiolites and labeled metamorphic olivine (e.g., Khalil and Azer, 2007; Gahlan et al., 2020; Ali et al., 2020).Metamorphic olivine in various ANS serpentinites has been attributed either to thermal effects of granitoid intrusions (e.g. Gahlan and Arai, 2009; Khalil and Azer,

2007; Ali et al., 2020) or to low-pressure high-temperature regional metamorphism (Gahlan et al., 2015, 2020). In the current case, sample 53 is the only sample with metamorphic olivine and was collected close to the contact with a younger granodiorite intrusion, so this is evidently a case of contact metamorphism.

7.3. Petrogenesis of rodingitic rocks

Rodingite is metasomatic rock, enriched relative to its protolith in CaO and depleted in silica and Na_2O.Ittypically contains hydrogarnet, diopside, vesuvianite and chlorite (e.g. Tsikouras et al., 2009). It commonly develops from small bodies of mafic rocks hosted within larger masses of serpentinized ultramafic rock (Coleman, 1977), leading to genetic hypotheses that assume a relationship between serpentinization and rodingitization. Specifically, fluids escaping from serpentinizing peridotite are Ca-rich and silica-poor; infiltration of such fluids into mafic rocks leads to rodingite formation (e.g. Bach et al., 2013).In principle, the occurrence of rodingite may therefore help to constrain the evolution of the ophiolitic sequences in which it is found (e.g., Dilek and Furnes, 2011). However, hypotheses differ concerning the timing and location of rodingite formation (e.g. Hatzipanagiotou and Tsikouras, 2001; Palandri and Reed, 2004; Bach and Klein, 2009; Tsikouras et al., 2009; Bach et al., 2013), leading to different implications for their host terranes. Rodingites might develop during low-temperature hydrothermal alteration such as ocean-floor metamorphism (e.g., Schandl et al., 1989; Frost et al., 2008) or, by contrast, at the comparatively higher temperatures associated with obduction of ultramafic rocks onto continental crust and development of a metamorphic sole (Mittwede and Schandl, 1992).

At Um Rashid, we see two clearly different types of rodingitic rocks that imply the operation of two different processes of rodingitization. One might sort hypotheses for explaining the difference into two general categories: (1) the same fluid may have interacted at the same time and *P-T-f*O_2 conditions with two mafic protoliths, different in their mineralogy and bulk chemistry, leading to different results; or (2) different fluids at may have interacted at different times with the same protoliths, under independent *P-T-f*O_2 conditions. We observe no superposition or inheritance relationships between the two types of rodingitic rocks, so any sequence of formation of the two types (including syncontemporaneous) is admissible.

True rodingite samples at Um Rashid are characterized by the mineral assemblage garnet + vesuvianite + diopside +chlorite ±actinolite ±prehnite. They are enriched in CaO, Fe_2O_{3t}, and MgO compared to common gabbros as well as relative to the rodingite-like samples, which instead are enriched in SiO_2, Al_2O_3, and K_2O (Fig. 9a).True rodingite is also strongly depleted in most incompatible trace elements, whereas rodingite-like rock is enriched in these elements (Figs. 9b, c). It is difficult to propose parent lithologies that would be found in the mantle section of an ophiolite sequence that are sufficiently different to drive such opposite results upon interaction with a common fluid at common conditions. The opposite sense of change of many elements and the absence of any evident spatial relationship between the two types of rodingitic rocks suggest that different processes rather than different protoliths is a more promising hypothesis from which to begin a discussion.

Typical rodingite has been associated with Ca-metasomatism of basic rocks during serpentinization either on the sea floor or in proximity to a subduction zone (Coleman, 1977: Tsikouras et al., 2009). During serpentinization, olivine with (Mg+Fe)/Si = 2breaks down to serpentine with (Mg+Fe)/Si ≤ 1.5. Hence, if there is excess hydrous fluid that escapes from

serpentinizing peridotite, it likely exports dissolved Mg^{2+}while being buffered to a low Si-activity as long as olivine remains in the assemblage. Reaction of such metasomatic fluids with mafic assemblages enriches them in MgO while leaching SiO_2 as the fluid adjusts towards equilibrium with a higher Si-activity (Tsikouras et al., 2009). The source of Ca is less obvious, since depleted peridotite is a poor source for Ca. What little Ca remained in the depleted peridotite after melt extraction might be effectively leached during serpentinization (no clinopyroxene survives the process), or it might have already been present in the source fluids before serpentinization and remained in solution. Or, Ca originally hosted in plagioclase in the mafic protoliths themselves may simply become passively enriched and incorporated into Ca-rich phases as a result of overall mass loss dominated by desilication (Frost et al., 2008).

The samples we have called rodingite-like rock, although light-colored and found apparently replacing mafic material within serpentinite, are not Ca-enriched. Rodingite-like rocks have the mineral assemblage hercynite (green spinel), preiswerkite, margarite, corundum, ferropargasite, plagioclase, clinozoisite and diaspore. In partly rodingitized samples, primary calcic plagioclase is albitized with rare relics of primary labradorite. Petrographic studies reveal that corundum and diaspore formed by replacement of green spinel; in partly rodingitized samples, corundum rims green spinel that becomes smaller and more irregular as the amount of diaspore and corundum increases. The reaction pathway from gabbro to highly replaced rodingite-like rock appears to involve early stabilization of green spinel driven by decreasing activity of CaO and $SiO_2$and increasing activity of Al_2O_3in high-temperature hydrothermal fluids (Nozaka et al., 2016). When the system reaches corundum saturation, Fe_2O_3 activity also begins to decrease. Desilication of plagioclase leads to the formation of margarite and muscovite (Bucher et al., 2005).

In rodingite-like samples, incompatible elements, notably LREE, Sr and Zr, are highly enriched. Enrichment increases from partly rodingitized samples (ΣREE 15-51 μg/g) to highly rodingitized samples (ΣREE 382-595μg/g). From a trace element perspective, these rocks do not look like gabbros at all. Highly enriched protoliths such as plagiogranites would be inconsistent with relict gabbroic minerals and textures in the partly rodingitized samples. Rather, we attribute the trace element enrichment to the effects of the extensive metasomatism that also modified the major-element chemistry. The increase of orders of magnitude in incompatible element concentration cannot be sensibly explained as residual concentration due to mass loss; it is necessary that most of the trace element enrichment represents addition from fluids. Except for the highest LOI sample (42), which is rich in secondary carbonates, the fluid-mobile element concentrations are well-correlated with LOI. However, high Zr and Hf in the rodingite-like rocks is challenging to explain with fluid addition; it requires growing zircons to sequester and concentrate these elements from hydrous fluids carrying Zr derived from a subducting slab or liberated by breakdown of olivine and pyroxene during serpentinization. Sr may be retained in the rodingite-like rock by growth of margarite, a phase often characterized by high Sr concentrations (Bucher et al., 2005).

Among the rodingite-like rocks, positive Eu anomalies are most developed in the least enriched and least rodingitized samples. The magnitude of the Eu anomaly in sample 42 resembles that seen in ophiolitic metagabbros in other Eastern Desert ophiolites (Gahlan et al., 2015). Hence, we interpret the positive Eu anomalies in the rodingite-like rocks as inherited from their plagioclase-rich protoliths (Hall and Ahmed, 1984). The anomaly is progressively overwhelmed by sequestration of all REE from fluids and loss of plagioclase from the assemblage.

Chloritite blackwall rims are found between rodingite and serpentinite at Um Rashid and other Eastern Desert localities (Takla et al., 1991, 2003; Abdel-Karim, 2000; Boskabadi et al., 2017). Chloritites may develop from ultramafic rocks by metasomatism or from pelitic sediments by low-grade metamorphism. In fact, various authors have assigned chloritite occurrences in the Eastern Desert to both metasedimentary (El-Ramly and Akaad, 1960) and ultramafic metasomatic scenarios (Takla et al., 1991; Abdel-Karim, 2000; Boskabadi et al., 2017).In the present study, there is little evidence within the chloritites themselves to indicate a protolith; there are no primary minerals or original textures. However, their occurrence in a transitional reaction zone between serpentinite and rodingite strongly suggests that they are metasomatic products developed from serpentinite during development of the adjacent rodingite.

7.4. Formation of mineral assemblages in the rodingitic rocks

The suite of minerals in the true rodingites at Um Rashid point consistently to temperatures of 300±100°C.Chlorite formation temperatures are 217-375°C.A key indicator phase for peak conditions in the rodingite assemblage is calcic garnet, both andradite and grossular. Grossular, especially hydrogrossular, may form after calcic plagioclase by plagioclase breakdown directly or via intermediary prehnite or clinozoisite (Schandl et al., 1989), by reaction with amphibole in the presence of excess CaO and water (Koutsovitis et al., 2013), or less commonly by reaction of clinopyroxene and plagioclase with excess water (Li et al., 2007).Enrichment in hydrogrossular component reflects the combination of high water activity and low silica activity (Frost and Beard, 2007). The reaction path models of Bach and Klein (2009), however, show that grossular develops at both 200 °C and 300°C but does not develop at 400°C, whereas clinozoisite is dominant at 300°C and absent at 200°C. Vesuvianite generally

forms in water-rich and very CO_2-poor fluids at 300-400°C (Hatzipanagiotou et al., 2003; Koutsovitis et al., 2013). Vesuvianite may develop by reaction of chlorite with hydrogrossular in the presence of excess Ca(Koutsovitis et al., 2013).Andradite is thought to grow directly from low-CO_2, high-pH, Fe-rich and Ca-rich fluids; the stability field for andradite is broad at 300°C and becomes increasing narrow, requiring specific combinations of intensive parameters, below 200 °C (Beard and Hopkinson, 2000). In combination, the assemblage of (hydro) grossular+(hydro) andradite+vesuvianite without clinozoisite in true rodingite samples appears to require temperatures close to but probably less than 300°C.

According to Bach and Klein (2009) and Bach et al. (2013), rodingite dykes often have a well-defined mineralogical zonation. Garnet is mostly found near the rims of dykes, whereas clinopyroxene and chlorite gradually increase inwards towards the cores, which are dominated by epidote, tremolite, prehnite and plagioclase. The core areas lack vesuvianite or calcite. This rim to core zonation is interpreted as a progression of decreasing water/rock ratio as fluids originally buffered by serpentinite move towards equilibrium with a gabbroic bulk chemistry. In the experiment of Palandri and Reed (2004),which used a pyroxene-bearing protolith reacting with a serpentinizing fluid rich in Al and Ca at 300°C and 100 bars, the mineral assemblages observed in sequence with decreasing water/rock ratio are the following: vesuvianite + chlorite + grossular → prehnite + grossular + chlorite → diopside + prehnite + grossular →diopside + prehnite→ diopside + prehnite + wairakite→prehnite + wairakite + chlorite. The present rodingite dykes sample the high water/rock ratio parts of this sequence, all containing vesuvianite and not reaching the appearance of wairakite.

The rocks we have described as rodingite-like have a very different mineral assemblage, consisting of hercynite, corundum±diaspore, plagioclase, aluminous micas, and clinozoisite.

Micas are mainly preiswerkite and margarite with subordinate muscovite. Petrographically, the micas appear to have formed at a late stage, after corundum and secondary sodic plagioclase. According to Godard and Smith (1999),margarite and preiswerkite suggest Na and Al-rich, silica-poor systems under greenschist facies conditions. Likewise, the development of albite suggests slower greenschist facies metamorphism of gabbro. Clinozoisite formed at the expense of calcic plagioclase. Rather than the Ca-rich fluids buffered by serpentinizing reactions that control the formation of true rodingite, the rodingite-like rocks are more likely the product of extreme leaching of mobile elements and retention of Al during seawater alteration (Hall and Ahmed, 1984). Evarts and Schiffman (1983) point specifically to seawater as the fluid source for similar Al-rich greenschist-facies metasomatism in the Del Puerto Ophiolite, California.

8. Summary

- The Um Rashid ophiolite is dismembered, strongly deformed, and metamorphosed. The outcrop is dominated by serpentinite, with less common metagabbro found as blocks of various sizes and shapes within ophiolitic mélange. Alteration mechanisms include serpentinization, carbonatization, listvenitization, rodingitization and silicification.
- Despite extensive replacement, fresh relics of primary chromian spinel, olivine and orthopyroxene are preserved in serpentinites. The chemistry of relict phases, together with preserved texture and whole-rock major and trace-element geochemical data, indicate protoliths of strongly depleted harzburgite and minor dunite. Mantle rocks residual to high degrees of partial melt extraction are typical of fore-arc supra-subduction zone oceanic lithosphere.
- One sample adjacent to a younger granodiorite intrusion contains metamorphic olivine.

- A suite of light-colored rocks within serpentinite and ophiolitic mélange is divided on the basis of field relations and mineral assemblages into typical rodingites and rodingite-like rock. True rodingite occurs as blocks and lenses in ophiolitic mélange with narrow chloritite blackwall rims. Rodingite-like rock forms thin dykes in serpentinite with, in some samples, remnants of gabbroic minerals and texture. Rodingite consists essentially of garnet, clinopyroxene, vesuvianite and chlorite with minor prehnite and opaque minerals. Rodingite-like rock consists essentially of corundum, hercynite, micas and plagioclase with minor secondary amphibole, clinozoisite, prehnite, diaspore and epidote.
- Typical rodingite is enriched in CaO, Fe_2O_3, MgO and compatible trace elements. Rodingite samples have low REE concentrations with nearly flat REE patterns and slight positive Ce anomalies. Rodingite-like rock, by contrast, shows enrichment in SiO_2, Al_2O_3,K_2O, and incompatible elements including Ba, Sr, Zn and Zr (but not Nb or Ta). Rodingite-like samples have widely variable REE patterns reaching considerable enrichment, with significant enrichment in LREE.
- The rodingite and rodingite-like rocks are both derived from gabbroic protoliths by interaction with different fluids, probably at different times during the evolution of the ophiolite. True rodingites likely developed at the boundaries of serpentinized peridotite and gabbroic units, driven by infiltration of Ca-bearing serpentinite-buffered fluids crossing into the gabbro and approaching equilibrium as water/rock ratios declined. The rodingite-like rocks, on the other hand, experienced strong Al enrichment through lower greenschist-grade interaction with seawater-derived fluids.

9. Acknowledgments

We acknowledge the National Research Centre (NRC), Egypt forlogistical support of this work. The present manuscript is a part of the master's thesis of Heba S. Mubarak (the first author). PDA is support by the US NSF, award 1947616. The authors are also indebted to the editor (Prof. Michael Roden) and two reviewers (Prof. Abdel-Aal M. Abdel-Karim and anonymous reviewer) for their efforts and numerous helpful comments.

10. References

Abdel-Karim, A.A., 2000. Chlorite schists and rodingites in the mafic-ultramafic rocks from the central Eastern Desert of Egypt: Petrogenesis and metamorphic history. M.E.R.C. Ain Shams University, Earth Science Series14, 150-170.

Abdel-Karim, A.A.M., El-Shafei, S.A., Azer, M.K., 2020. The Neoproterozoic ophiolitic ultramafic rocks in Eastern Desert of Egypt: implications for petrogenesis and metasomatic processes. International Geology Review, pp.1-25.

Ali, R., Pitcairn, I., Maurice, A., Azer, M.K., Bakhit, B., Shahien, M., 2020. Petrology and geochemistry of ophiolitic ultramafic rocks and chromitites across the Eastern Desert of Egypt: Insights into the composition and nature of a Neoproterozoic mantle and implication for the evolution of SSZ system. Precambrian Research 337,105565.

Arif, M., Jan, M.Q., 2006. Petrotectonic significance of the chemistry of chromite in the ultramafic-mafic complexes of Pakistan. Journal of Asian Earth Sciences 27, 628-646.

Azer, M.K., 2014. Petrological studies of Neoproterozoic serpentinized ultramafics of the Nubian Shield: Spinel compositions as evidence of the tectonic evolution of the Egyptian ophiolites. Acta Geologica Polonica 64, 113–127.

Azer, M.K., Stern, R.J., 2007. Neoproterozoic (835-720 Ma) serpentinites in the Eastern Desert, Egypt: Fragments of fore-arc mantle. The Journal of Geology 115, 457–472.

Bach, W., Jöns, N., Klein, F., 2013. Metasomatism within the Ocean Crust. Metasomatism and the Chemical Transformation of Rock. Springer, Berlin Heidelberg,253–288.

Bach, W., Klein, F., 2009. The petrology of seafloor rodingites: Insights from geochemical reaction path modeling. Lithos 112, 103-117.

Barnes, S.J., 2000. Chromite in komatiites, II. Modification during greenschist to mid-amphibolite facies metamorphism. Journal of Petrology 41(3), 387-409.

Barnes, S.J., Roeder, P.L., 2001. The range of spinel compositions in terrestrial mafic and ultramafic rocks. Journal of Petrology 42, 2279–2302.

Beard, J.S., Hopkinson, L., 2000. A fossil, serpentinization-related hydrothermal vent, Ocean Drilling Program Leg 173, Site 1068 (Iberia Abyssal Plain): Some aspects of mineral and fluid chemistry. Journal of Geophysical Research: Solid Earth, 105(B7), pp.16527-16539.

Bell, J., Clark, E., Marshall, P., 1911. The geology of the Dun Mountain subdivision, Nelson. New Zealand Geological Survey Bulletin 12, 1-71.

Bloomer, S., Taylor, B., MacLeod, C., Stern, R., Fryer, P., Hawkins, J., Johnson, L., 1995. Early arc volcanism and ophiolite problem: A perspective from drilling in the Western Pacific. In: Taylor, B., Natland, J. (Eds.),Active Margins and Marginal Basins of the Western Pacific, Geophysical Monograph, Vol. 88. American Geophysical Union, Washington, DC, pp. 1-30.

Boedo, F., Escayela, M., PerezLujan, S., Vajovich, G.,Ariza, J., Naipauer, M., 2015.Geochemistry of Precordillera serpentinites, Western Argentina: evidence for

multistage hydrothermal alteration and tectonic implications for the Neoproterozoic-early Paleozoic. Geologica Acta 13 (4), 263-278.

Bonatti, E., Michael, P.J., 1989. Mantle peridotites from continental rifts to oceanic basins to subduction zones. Earth and Planetary Science Letters 91, 297-311.

Boskabadi, A., Pitcairn, I., Broman, C., Boyce, A., Teagle, D., Cooper, M., Azer, M., Mohamed, F., Stern, R., Majka, J., 2017. Carbonate alteration of ophiolitic rocks in the Arabian–Nubian Shield of Egypt: sources and compositions of the carbonating fluid and implications for the formation of Au deposits. International Geology Review 59(4), 391–419.

Bucher, K., DeCapitani, C., Grapes, R., 2005. The development of margarite-corundum blackwall by metasomatic alteration of a slice of mica schist in ultramafic rock, Kvesjoen, Norwegian Caledonides. Canadian Mineralogist 43,129-156.

Cardenas-Párraga, J., García-Casco, A., Proenza, J., Harlow, G., Blanco-Quintero, I., Lázaro, C., Villanova-de-Benavent, C. and Núñez Cambra, K., 2017. Trace-element geochemistry of transform-fault serpentinite in high-pressure subduction mélanges (eastern Cuba): Implications for subduction initiation. International Geology Review 59(16), 2041-2064.

Cathelineau, M., Nieva, D., 1985.A chlorite solid solution geothermometer. The Los Azufrez (Mexico) geothermal system. Contributions to Mineralogy and Petrology 91, 235–244.

Coleman, R.G., 1977. Ophiolites, Ancient Oceanic Lithosphere? Springer-Verlag, Berlin, pp. 1-229.

Deschamps, F., Godard, M., Guillot, S., Hattori, K., 2013. Geochemistry of subduction zone serpentinites: a review. Lithos 178, 96–127.

Dick, H.J., Bullen, T., 1984.Chromian spinel as a petrogenetic indicator in abyssal and alpine-type peridotites and spatially associated lavas. Contributions to Mineralogy and Petrology 86(1), 54-76.

Dilek, Y., Furnes, H., 2011. Ophiolite genesis and global tectonics: Geochemical and tectonic fingerprinting of ancient oceanic lithosphere. Geological Society of America Bulletin 123(3-4), 387-411.

El-Ramly, M.F., Akaad, M.K., 1960. The basement complex in the Central Eastern Desert. Geological Survey of Egypt8, 35p.

El Sharkawy, M.A., El Bayoumi, R.M., 1979. The ophiolites of Wadi Ghadir area, Eastern Desert, Egypt. Annals of the Geological Survey of Egypt 9, 125-135.

Evans, B.W., 2010. Lizardite versus antigorite serpentinite: magnetite, hydrogen, and life (?). Geology 38, 879-882.

Evarts, R.C., Schiffman, P., 1983. Submarine hydrothermal metamorphism of the Del Puerto ophiolite, California. American Journal of Science 283(4), 289-340.

Evensen, N., Hamilton, P., O'Nions, R., 1978. Rare earth abundances in chondritic meteorites. Geochimica et Cosmochimica Acta 42(8), 1199-1212.

Frost, B.R., Beard, J.S., 2007. On silica activity and serpentinization. Journal of Petrology 48, 1351-1368.

Frost, R., Beard, J., McCaig, A., 2008. The formation of micro-rodingites from IODP Hole U1309D: Key to understanding the process of serpentinization. Journal of petrology 49 (9), 1579-1588.

Gahlan, H., Arai, S., 2009. Carbonate-orthopyroxenite lenses from the Neoproterozoic Gerf ophiolite, South Eastern Desert, Egypt: The first record in the Arabian Nubian Shield ophiolites. Journal of African Earth Sciences 53,70-82

Gahlan, H., Azer, M., Khalil, A., 2015.The Neoproterozoic Abu Dahr ophiolite, South Eastern Desert, Egypt: Petrological characteristics and tectonomagmatic evolution. Mineralogy and Petrology 109, 611-630.

Gahlan, H., Azer, M., Asimow, P., Mubarak, H., Al-Kahtany, K., 2020. Petrological characteristics of the Neoproterozoic Ess ophiolite mantle section, Arabian Shield, Saudi Arabia: a mineral chemistry perspective. International Journal of Earth Sciences 109, 239-251.

Gamal El Dien, H.G., Arai, S., Doucet, L.S., Li, Z.X., Kil, Y., Fougerouse, D., Reddy, S.M., Saxey, D.W. and Hamdy, M., 2019. Cr-spinel records metasomatism not petrogenesis of mantle rocks. Nature communications 10(1), 1-12.

Garson, M.S., Shalaby, I.M., 1976. Precambrian-Lower Paleozoic plate tectonics and metallogenesis in the Red Sea region. Geological Association of Canada, Special Paper No. 14.

Girardeau, J., Mevel, C., 1982. Amphibolitized sheared gabbros from ophiolites as indicators of the evolution of the oceanic crust: Bay of islands, Newfoundland. Earth and Planetary Science Letters 61, 151-165.

Godard, G., Smith, D., 1999. Preiswerkite and Na-(Mg, Fe)-margarite in eclogites. Contributions to Mineralogy and Petrology 136(1-2), 20-32.

Godard, M., Lagabrielle, Y., Alard, O., Harvey, J., 2008. Geochemistry of the highly depleted peridotite drilled at ODP Sites 1272 and 1274 (Fifteen –Twenty Fracture Zone, Mid-

Atlantic Ridge): implication from mantle dynamics beneath a slow spreading ridge. Earth and Planetary Science Letters 276,410-425.

Hall, A., Ahmed, Z., 1984. Rare earth content and origin of rodingites. Chemie der Erde 43(1), 28-51.

Hart, S.R., Zindler, A., 1986. In search of a bulk-Earth composition. Chemical Geology 57(3-4),247-267.

Hatzipanagiotou, K., Tsikouras, B., 2001. Rodingite formation from diorite in the Samothraki ophiolite NE Aegean, Greece. Geological Journal 36, 93-109.

Hatzipanagiotou, K., Tsikouras, B., Migiros, G., Gartzos, E., Serelis, K., 2003. Origin of rodingites in ultramafic rocks from Lesvos island (NE Aegean, Greece). Ofioliti 28, 13–23.

Hey, M. H., 1954.A new review of the chlorites.Mineralogical Magazine 30, 272-292.

Hirose, K., Kawamoto, T., 1995. Hydrous partial melting of lherzolite at 1GPa: the effect of H2O on the genesis of basaltic magmas. Earth and Planetary Science Letters 133, 463-473.

Hussein, A.A., Mazhar, A.A., Smith, M., Masoud, M.S., Hkyamy, M.S., Hamouda, E.M., 1994. Geological map of Ghadir-Dunqash district, Eastern Desert, Egypt. Geological Survey of Egypt.

Ishii, T., Robinson, P.T., Maekawa, H., Fiske, R., 1992. Petrological studies of peridotites from diapiric Serpentinite Seamounts in the Izu- Ogasawara-Mariana forearc, leg 125. In: J. Pearce, L.B. Stokking, et al. (Eds.), Proceedings of the Ocean Drilling Project, Leg 125, Scientific Results (College Station), pp. 445-485.

Ishimaru, S., Arai, S., Ishida, Y., Shirasaka, M., Okrugin, V. M., 2007. Melting and multi-stage metasomatism in the mantle wedge beneath a frontal arc inferred from highly depleted peridotite xenoliths from the Avacha volcano, southern Kamchatka. Journal of Petrology, 48, 395-433.

Jagoutz, E., Palme, H., Baddenhausen, H., Blum, K., Cendales, M., Dreibus, G., Spettel, B., Lorenz, V., Vanke, H., 1979. The abundance of major, minor and trace elements in the earth's mantle as derived from primitive ultramafic nodules. Geochimica et Cosmochimica Acta 11, 2031–2050.

Keusen, H. R., Peters, T., 1980. Preiswerkite, an Al-rich trioctahedral sodium mica from the Geisspfad ultramafic complex (Penninic Alps). American Mineralogist 65, 1134-1137.

Keeditse, M. Rajesh, H.M., Belyanin, G.A., Fukuyama, M., Tsunogae, 2016.Primary magmatic amphibole in Archaean meta-pyroxenite from the central zone of the Limpopo Complex, South Africa. South African Journal of Geology 119(4), 607-622.

Khalil, A.E.S., Azer, M.K., 2007. Supra subduction affinity in the Neoproterozoic serpentinites in the Eastern Desert, Egypt: evidence from mineral composition. Journal of African Earth Sciences 49, 136–152.

Koutsovitis, P., 2017. High-pressure subduction-related serpentinites and metarodingites from East Thessaly (Greece): Implications for their metamorphic, geochemical and geodynamic evolution in the Hellenic–Dinaric ophiolite context. Lithos 276, 122-145.

Koutsovitis, P., Magganas, A., Pomonis, P., Ntaflos, T., 2013. Subduction-related rodingites from East Othris, Greece: mineral reactions and physicochemical conditions of formation. Lithos 172-173.

Kranidiotis, P., MacLean, W.H., 1987. The systematics of chlorite alteration at the Phelps Dodge massive sulfide deposit, Matagami, Quebec. Economic Geology 82, 1898–1911.

Leake, B.E., Woolley, A.R., Arps, C.E.S., Birch, W.D., Gilbert, M. C., Grice, J.D., Hawthorne, F.C., Kato, A., Kisch, H. J., Krivovichev, V.G., Linthout, K., Laird, J., Mandarino, J., Maresch, W.V., Nickel, E.H., Rock, N.M.S., Schumacher, J.C., Smith, D.C., Stephenson, N.C.N., Ungaretti, L., Whittaker,E.J.W., Youzhi, V., 1997. Nomenclature of amphiboles: Report of the Subcommittee on Amphiboles of the International Mineralogical Association Commission on New Minerals and Mineral Names. Mineralogical Magazine 61, 295-321.

Li, X., Zhang, L.,Wei, C., Ai, Y., Chen, J., 2007. Petrology of rodingite derived fromeclogite in western Tianshan, China. Journal of Metamorphic Geology 25, 363–382.

McDonough, W.F., Sun, S.S., 1995. The Composition of the Earth.Chemical Geology 120, 223–53.

Mittwede, S.K., Schandl, E.S., 1992. Rodingites from the Southern Appalachian piedmont, South Carolina, USA. European Journal of Mineralogy 4 (1), 7-16.

Mogahed, M.M., Saad, W.M., 2020. Geotectonic significance of the Neoproterozoic ophiolitic metagabbros of Muiswirab area, South Eastern Desert, Egypt: constraints from their mineralogical and geochemical characteristics. *Acta Geochimica* (https://doi.org/10.1007/s11631-020-00404-8).

Morimoto, N., Fabries, J., Ferguson, A., Ginzburg, I., Ross, M., Seifert, F., Zussman, J., Aoki, K., Gottardi, G., 1988.Nomenclature of pyroxenes. Mineralogical Magazine 52, 535–550.

Niu, Y., 2004. Bulk-rock major and trace element compositions of abyssal peridotites: implications for mantle melting, melt extraction and post-melting processes beneath mid-ocean ridges. Journal of Petrology 45, 2423–2458.

Nozaka, T., 2003. Compositional heterogeneity of olivine in thermally metamorphosed serpentinite from southwest Japan. American Mineralogist 88, 1377–1384.

Nozaka, T., Meyer, R., Wintsch, R., Wathen, B., 2016.Hydrothermal spinel, corundum and disapore in lower oceanic crustal troctolites from the Hess Deep Rift.Contribution to Mineralogy and Petrology171, 53.

Ohara, Y., Stern, R., Ishii, T., Yurimoto, H., Yamazaki, T., 2002. Peridotites from the Mariana Trough: first look at the mantle beneath an active back-arc basin. Contribution to Mineralogy and Petrology 143, 1-18.

Pagé, P., Bédard, J., Schroetter, J., Tremblay, A., 2008. Mantle petrology and mineralogy of the Thetford Mines ophiolite complex. Lithosphere 100, 255–292.

Palandri, J.L., Reed, M.H., 2004. Geochemical models of metasomatism in ultramafic systems: Serpentinization, rodingitization, and sea floor carbonate chimney precipitation. Geochimica et Cosmochimica Acta 68 (5), 1115-1133.

Parkinson, I.J., Pearce, J.A., 1998. Peridotites from the Izu-Bonin-Mariana forearc (ODP Leg 125): Evidence for mantle melting and melt-mantle interaction in a supra-subduction zone setting. Journal of Petrology 39, 1577–1618.

Paulick, H., Bach, W., Godard, M., De Hoog, J.C.M., Suhr, G. Harvey, J., 2006. Geochemistry of abyssal peridotites (Mid-Atlantic Ridge, 15 20′ N, ODP Leg 209): implications for fluid/rock interaction in slow spreading environments. Chemical geology 234(3-4), 179-210.

Pearce, J., Barker, P., Edwards, S., Parkinson, I., Leat, P., 2000.Geochemistry and tectonic significance of peridotites from the South Sandwich arc-basin system, South Atlantic. Contributions to Mineralogy and Petrology 139, 36–53.

Petriglieri, J. R., Salvioli-Mariani, E., Mantovani, L., Tribaudino, M., Lottici, P. P., Laporte-Magoni, C., Bersani, D., 2015.Micro-Raman mapping of the polymorphs of serpentine. Journal of Raman Spectroscopy 46, 953-958.

Scambelluri, M., Cannao, E., Gilio, M., 2019. The water and fluid-mobile element cycles during serpentinite subduction. A review.European Journal of Mineralogy 31,405-428.

Schandl, E., O'Hanely, D., Wicks, F., 1989. Rodingites in serpentinized ultramafic rocks of the Abitibi greenstone belt, Ontario. Canadian Mineralogist 27, 579-591.

Shackleton, R.M., 1994. Review of late Proterozoic sutures, ophiolitic mélanges and tectonics of eastern Egypt and northeastern Sudan. Geologische Rundschau 83, 537–546.

Stern, R., Johnson, P., Kröner, A., Yibas, B., 2004. Neoproterozoic ophiolites of the Arabian-Nubian Shield. In: Kusky, T.M. (Ed.), Precambrian Ophiolites and Related Rocks. Developments in Precambrian Geology 13, 95–128. Amsterdam: Elsevier.

Surour, A.A., 2019. Mid-ocean ridge vs. forearc and subduction settings: Clues from rodingitization of tectonic fragments in the Neoproterozoic ophiolites of the Eastern Desert, Egypt. Lithos 342, 18-30.

Takahashi, E., Uto, K., Schilling, J., 1987. Primary magma compositions and Mg/Fe ratios of their mantle residues along mid-Atlantic ridge 29N to 73N Technical Report, A9. Institute of Studies Earth's Interior, Okayama University Series, pp.1-14.

Takla, M.A., Basta, F.F., Surour, A.A., 1991. Chloritites at the contacts of some ophiolitic ultramafics, Eastern Desert, Egypt. Egyptian Mineralogist 3, 151-165.

Takla, M.A., Basta, F.F, Surour, A.A., 1992. Petrology and Mineral chemistry of rodingites associating the Pan-African ultramafics of Sikait-Abu Rusheid area, south Eastern Desert, Egypt. Geology of the Arab World, Cairo University 1, 492-507.

Takla, M.A., Trommsdorff, V., Basta, F.F., Surour, A.A., 2003. Margarite in ultramafic alteration zones (Blackwall): A new occurrence in Barramiya Area, Egypt. European Journal of Mineralogy 15(6), 991-999.

Tsikouras, B., Sofia Karipi, S., Rigopoulos, I., Perraki, M., Pomonis, P., Hatzipanagiotou, K., 2009. Geochemical processes and petrogenetic evolution of rodingite dykes in the ophiolite complex of Othrys (Central Greece). Lithos 113, 540-554.

Uysal, I., Ersoy, E., Dilek, Y., Kapsiotis, A., Sarıfakıoğlu, E., 2016. Multiple episodes of partial melting, depletion, metasomatism and enrichment processes recorded in the heterogeneous upper mantle sequence of the Neotethyan Eldivan ophiolite, Turkey. Lithos 246, 228-245.

Xiong, F., Yang, J., Dilek, Y., Wang, C., Hao, X., Xu, X., Lian, D., 2018. Petrology and geochemistry of the high-Cr podiform chromitites of the Köycegiz ophiolite, southwest Turkey: implications for the multistage evolution of the oceanic upper mantle. Mineralogy and Petrology 112, 685 –704.

Caption of Figures

Figure 1. Distribution of ophiolitic rocks in Eastern Desert of Egypt (modified after Shackleton, 1994). Location of the study area (Fig. 2) is indicated.

Figure 2. Geological map of the Um Rashid area (after Hussein et al., 1994). Sampling locations are indicated by stars with sample numbers.

Figure 3. Field photos and outcrop sketches from the Um Rashid area: (a) low-angle thrust contact between hanging-wall ophiolite and foot-wall volcano-sedimentary island-arc succession; (b) metagabbro block within ophiolitic mélange; (c) massive serpentinites; (d) foliated and brecciated sheared serpentinite; (e)talc-carbonate block within ophiolitic mélange; (f) rodingite block within ophiolitic mélange; (g) sketch showing the a rodingite block with chloritite blackwall hosted by ophiolitic mélange; (h) a dyke of rodingite-like rock within serpentinite; (i) sketch of a dyke of rodingite-like rock with gabbro remnants hosted by serpentinite; and (j) hand-sample of variably altered rodingite-like rock with remnant gabbroic texture.

Figure 4. Photomicrographs showing petrographic textures in the serpentinite. All photos are taken in cross-polarized transmitted light, except panel (c) is an electron backscatter image:(a) bastite texture in serpentine after orthopyroxene; (b) mesh texture after olivine with chrysotile veinlets; (c) chromian spinel crystals replaced by ferritchromite and Cr-magnetite at rims and along cracks; (d) fresh relics of primary olivine dissected by network veins of serpentine; (e) exsolved pyroxene showing metamorphic foliation and lineation; (f) sheared serpentinite showing subparallel alignment of serpentine flakes.

Figure 5. Photomicrographs showing petrographic textures in the rodingite. Panels (a), (b), (c) and (d)are back-scattered electron images; panels(e) and (f) are taken in plane-polarized transmitted light: (a) dissected garnet crystals transformed along the margins into chlorite; (b) diopside and garnet replaced along the margins by chlorite; (c) vesuvianite and diopside replaced along the margins by chlorite; (d) vesuvianite corroded and replaced by chlorite; (e) red crystals of rutile associated with opaque minerals; and (f) anhedral aggregate of corundum.

Figure 6. Photomicrographs showing petrographic textures in the rodingite-like rock. (a) and (c) are backscatter images, (b) is taken in plane-polarized transmitted light and (d) is taken in cross-polarized transmitted light:(a) corundum crystals associate with hercynite and preiswerkite; (b) green spinel (hercynite) surround by corundum and preiswerkite; (c) micas including preiswerkite and margarite associated with hercynite and diaspore; and (d) plagioclase showing albite twining.

Figure 7. Classification diagrams based on mineral chemistry in the Um Rashid suite:(a)pyroxenes (Morimoto et al, 1988); (b) primary and secondary amphiboles (Keeditse et al., 2016); (c) chlorite-group minerals (Hey, 1954); and (d) spinel-group minerals (Barnes and Röeder, 2001).

Figure 8. Whole-rock chemistry of serpentinites from Um Rashid: (a) nomenclature based on Ol-Opx-Cpx normative composition (after Coleman, 1977); (b) primitive mantle-normalized trace elements patterns (normalization values from McDonough and Sun, 1995); (c) chondrite-normalized rare earth element patterns (normalization values from Evensen et al., 1978).

Figure 9. Whole-rock chemistry of rodingite from Um Rashid: (a) Al_2O_3-CaO-Fe_2O_3 ternary diagram (Coleman, 1977); (b) Primitive mantle-normalized trace elements patterns(normalization values from McDonough and Sun, 1995); (c) Chondrite-normalized rare earth element patterns(normalization values from Evensen et al., 1978).

Figure 10. Tectonic classification of serpentinite by whole-rock chemistry:(a) Al_2O_3vs. CaO showing fields of Ishiiet al. (1992); (b)MgO/SiO_2vs.Al_2O_3/SiO_2 diagram showing fields ofabyssal peridotite (Niu, 2004), fore-arc peridotite(Pearce et al., 2000; Parkinson and Pearce (1998), and the terrestrial array (Jagoutz et al., 1979; Hart and Zindler, 1986).

Figure11. Tectonic discrimination diagrams for peridotites based on mineral chemistry: (a) Cr# vs. Mg# diagram for fresh chromian spinels (after Stern et al. 2004) with field boundaries are from Dick and Bullen (1984), Bloomer et al. (1995) and Ohara et al. (2002) and trend of experimental equilibrium melting in wt.% from Hirose and Kawamoto (1995); (b) Al_2O_3 vs. Cr_2O_3 in orthopyroxene;(c) Al_2O_3 vs. Mg# in orthopyroxene. Compositional fields for orthopyroxene adopted from Pagé et al. (2008) and Xiong et al. (2018).

Figure 12. Schematic tectonic model of Arabian-Nubian Shield fore-arc ophiolite development after Abdel-Karim et al. (2020): (a) opening of Mozambique ocean between East and West Gondwana; (b) subduction initiation or incipient arc stage, in which partial melting occurred in the mantle wedge and proto-fore-arc spreading begins over the subduction zone; (c) true subduction or mature-arc stage associated with high flux of slab-derived fluids that induce partial melting of pre-depleted mantle to yield boninitic melts.

Declaration of interests

☒ The authors declare that they have no known competing financial interests or personal relationships that could have appeared to influence the work reported in this paper.

☐The authors declare the following financial interests/personal relationships which may be considered as potential competing interests:

Highlights

- Rodingites are recorded within serpentinized ultramafics and ophiolitic mélange
- The protoliths of the ultramafic rocks were harzburgite with minor dunite
- Two types of rodingites are recognized: typical rodingite and rodingite-like rock
- The first stage of rodingitization was related with serpentinization of the peridotites
- The second stage of rodingitization occurred during obduction of the ophiolite

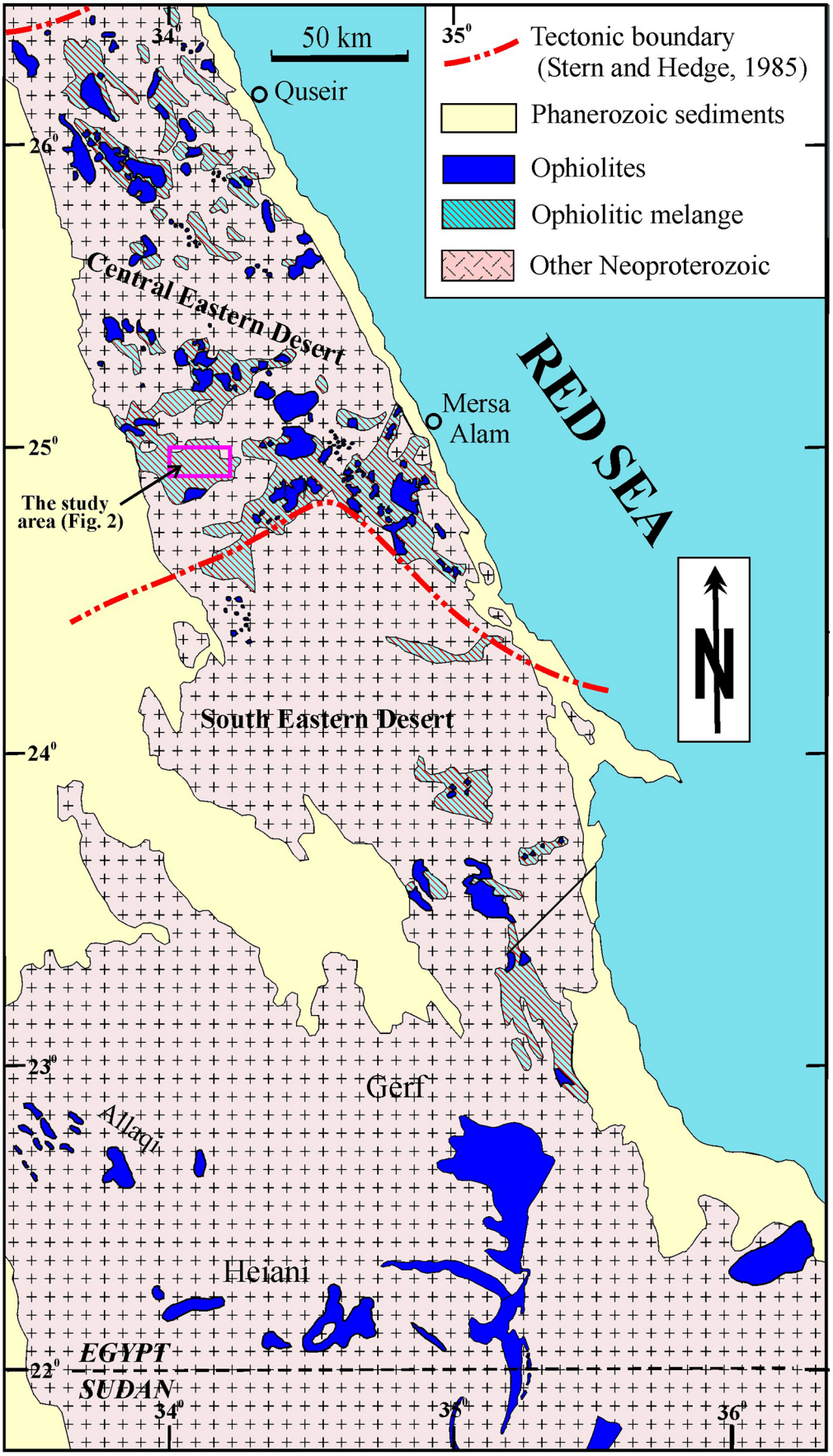
50 km
Quseir
Mersa Alam
RED SEA
Central Eastern Desert
South Eastern Desert
The study area (Fig. 2)
Gerf
Allaqi
Heiani
EGYPT
SUDAN
N
Tectonic boundary (Stern and Hedge, 1985)
Phanerozoic sediments
Ophiolites
Ophiolitic melange
Other Neoproterozoic
34°
35°
36°
26°
25°
24°
23°
22°

Figure 1

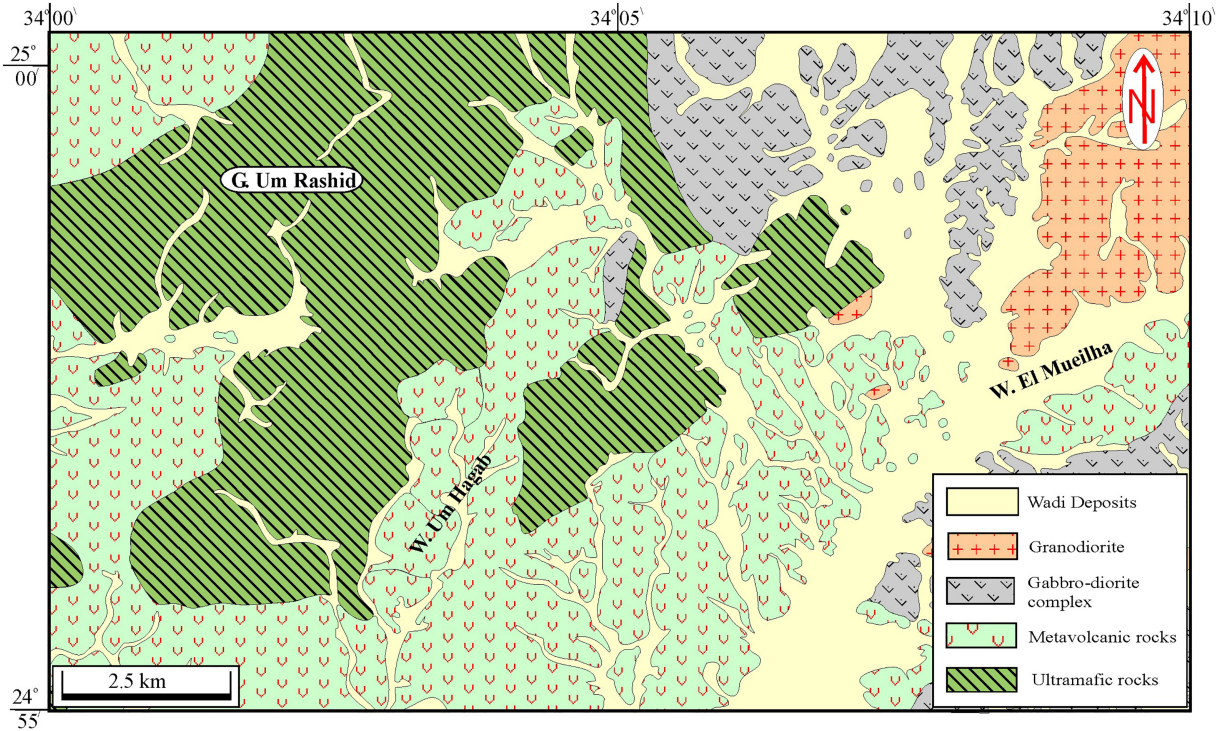
34°00'
34°05'
34°10'
25°00'
24°55'
G. Um Rashid
W. Um Hagab
W. El Mueilha
N
2.5 km
Wadi Deposits
Granodiorite
Gabbro-diorite complex
Metavolcanic rocks
Ultramafic rocks

Figure 2

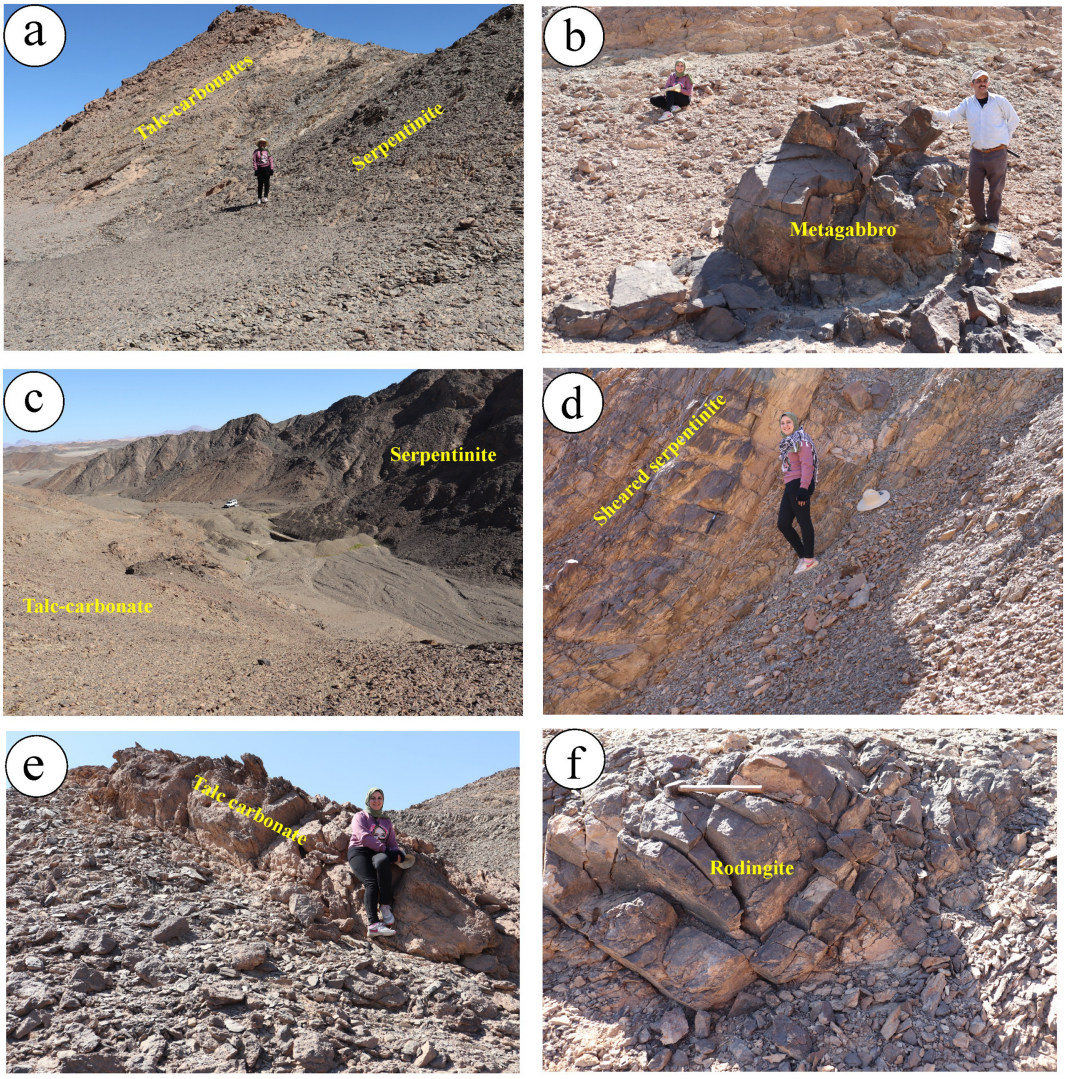
a
Talc-carbonates
Serpentinite
b
Metagabbro
c
Serpentinite
Talc-carbonate
d
Sheared serpentinite
e
Talc carbonate
f
Rodingite

Figure 3A

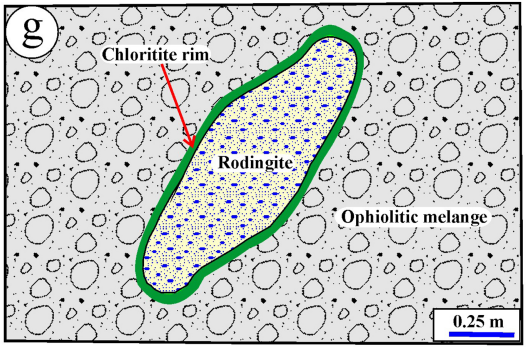
g
Chloritite rim
Rodingite
Ophiolitic melange
0.25 m

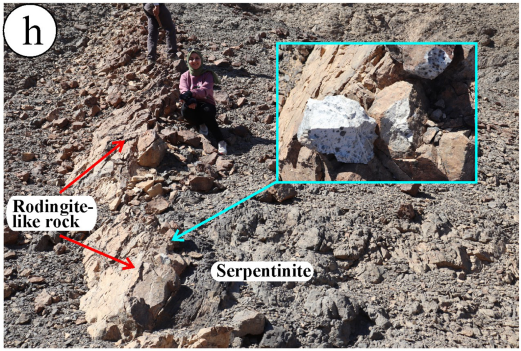
h
Rodingite-like rock
Serpentinite

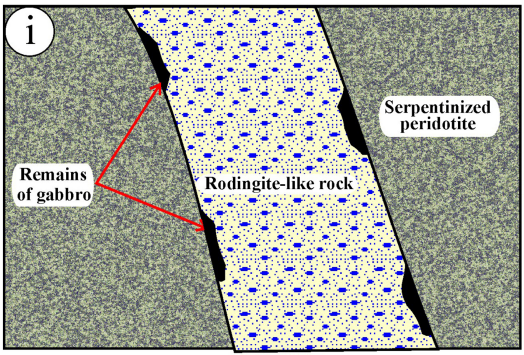
i
Remains of gabbro
Rodingite-like rock
Serpentinized peridotite


j
Rodingite-like rock
Gabbro with minor rodingitization

Figure 3B

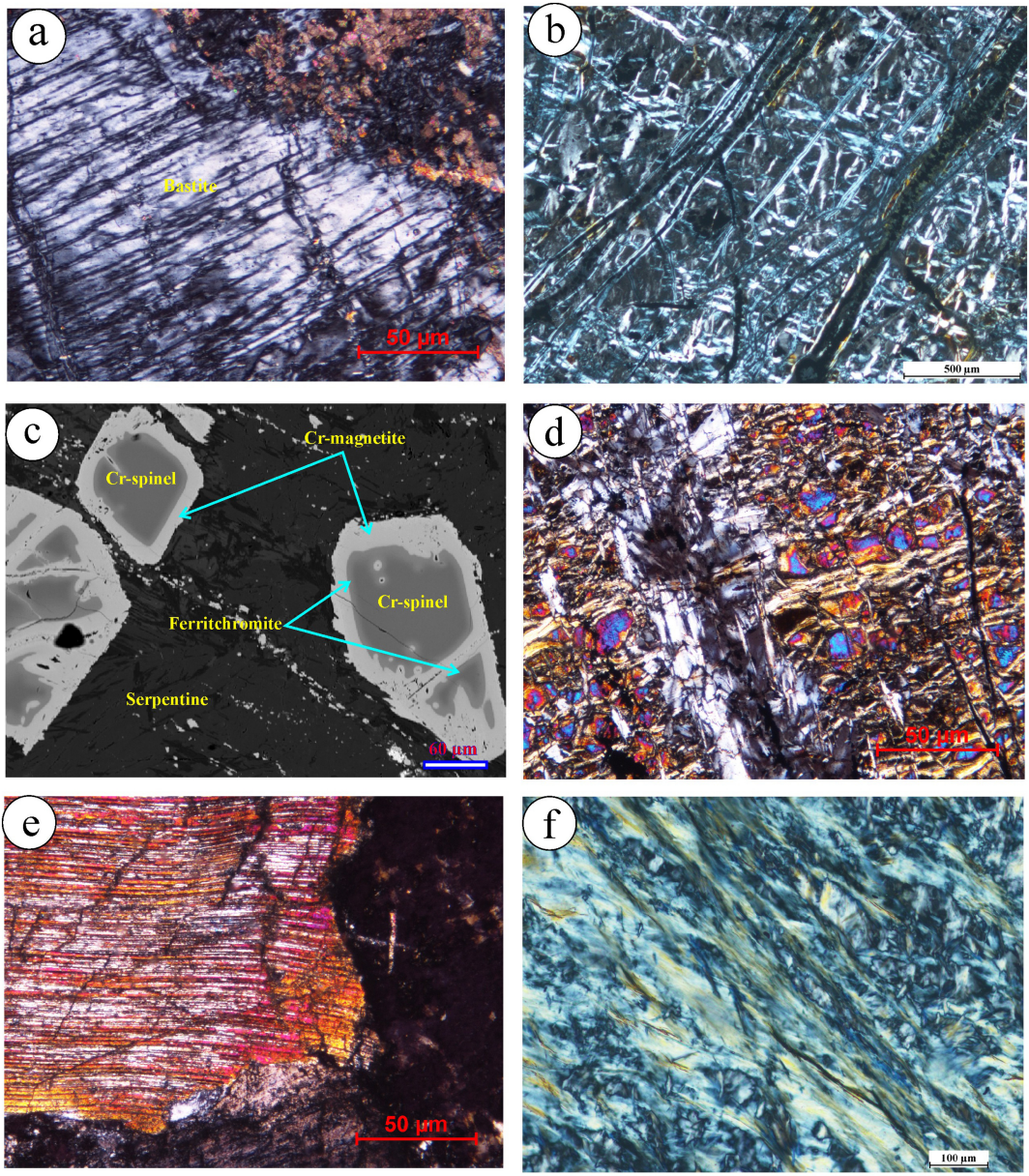
a
Bastite
50 µm
b
500 µm
c
Cr-magnetite
Cr-spinel
Cr-spinel
Ferritchromite
Serpentine
60 µm
d
50 µm
e
50 µm
f
100 µm

Figure 4

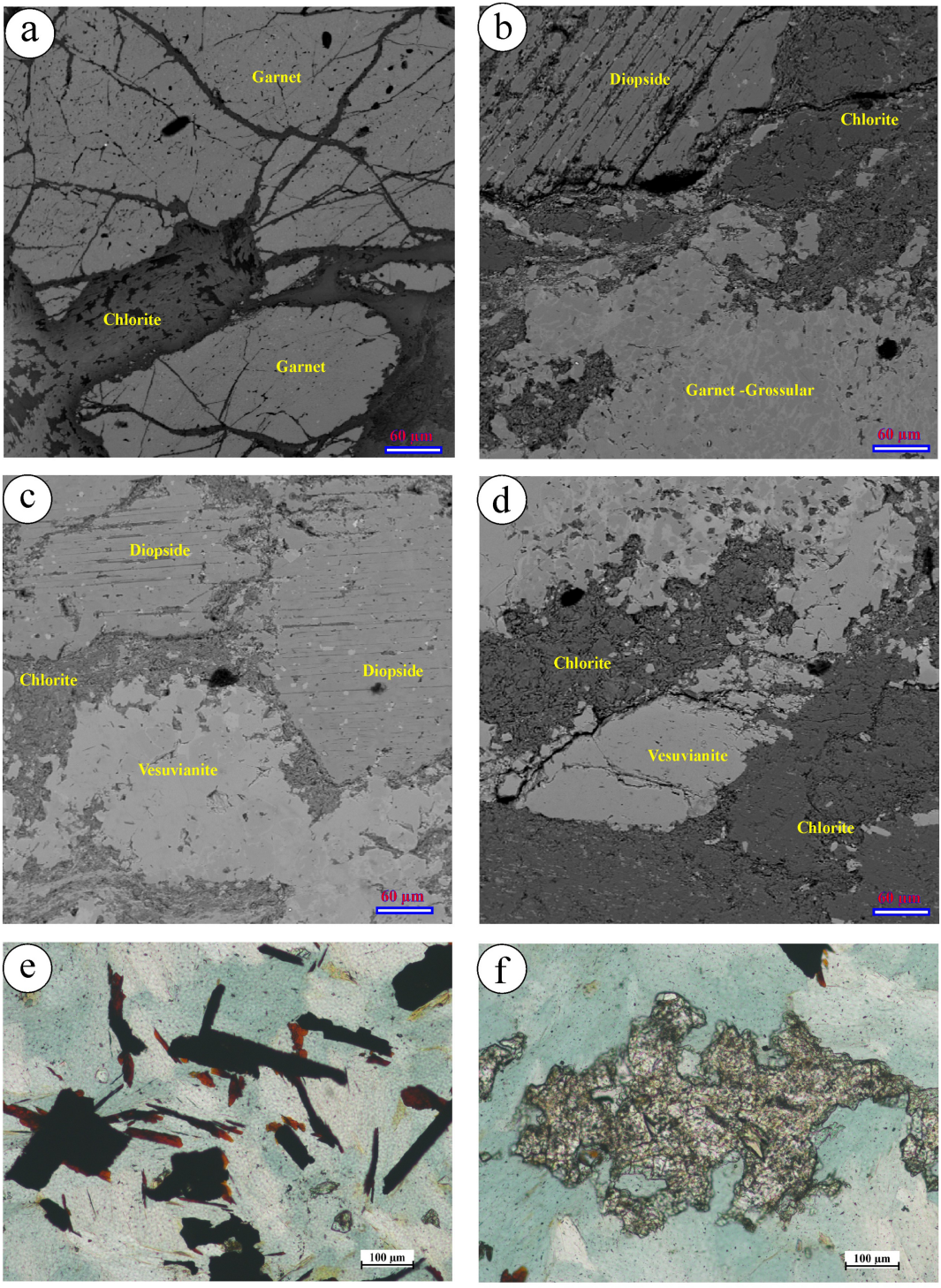
a
Garnet
Chlorite
Garnet
60 µm
b
Diopside
Chlorite
Garnet -Grossular
60 µm
c
Diopside
Chlorite
Diopside
Vesuvianite
60 µm
d
Chlorite
Vesuvianite
Chlorite
60 µm
e
100 µm
f
100 µm

Figure 5

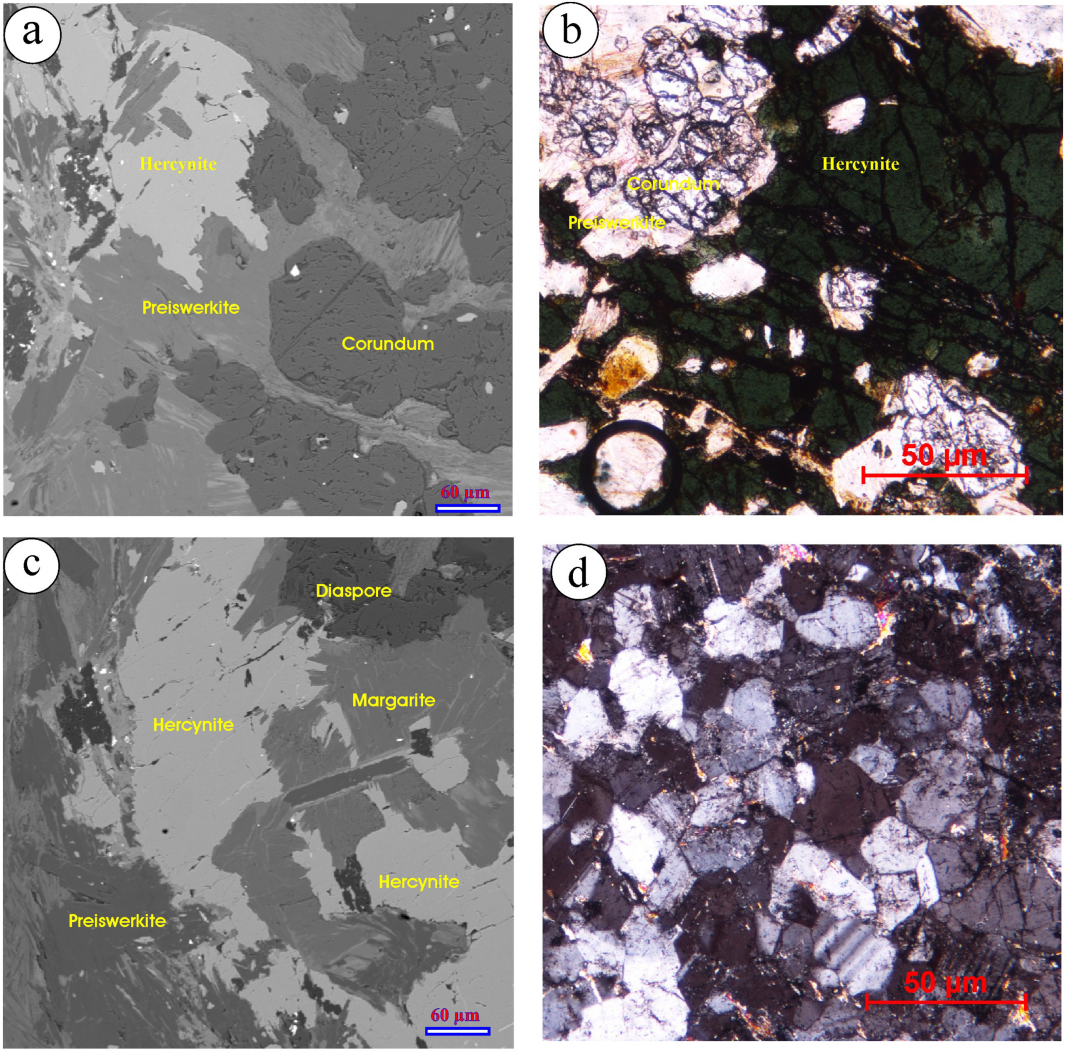
a
Hercynite
Preiswerkite
Corundum
60 μm
b
Hercynite
Corundum
Preiswerkite
50 μm
c
Diaspore
Margarite
Hercynite
Hercynite
Preiswerkite
60 μm
d
50 μm

Figure 6

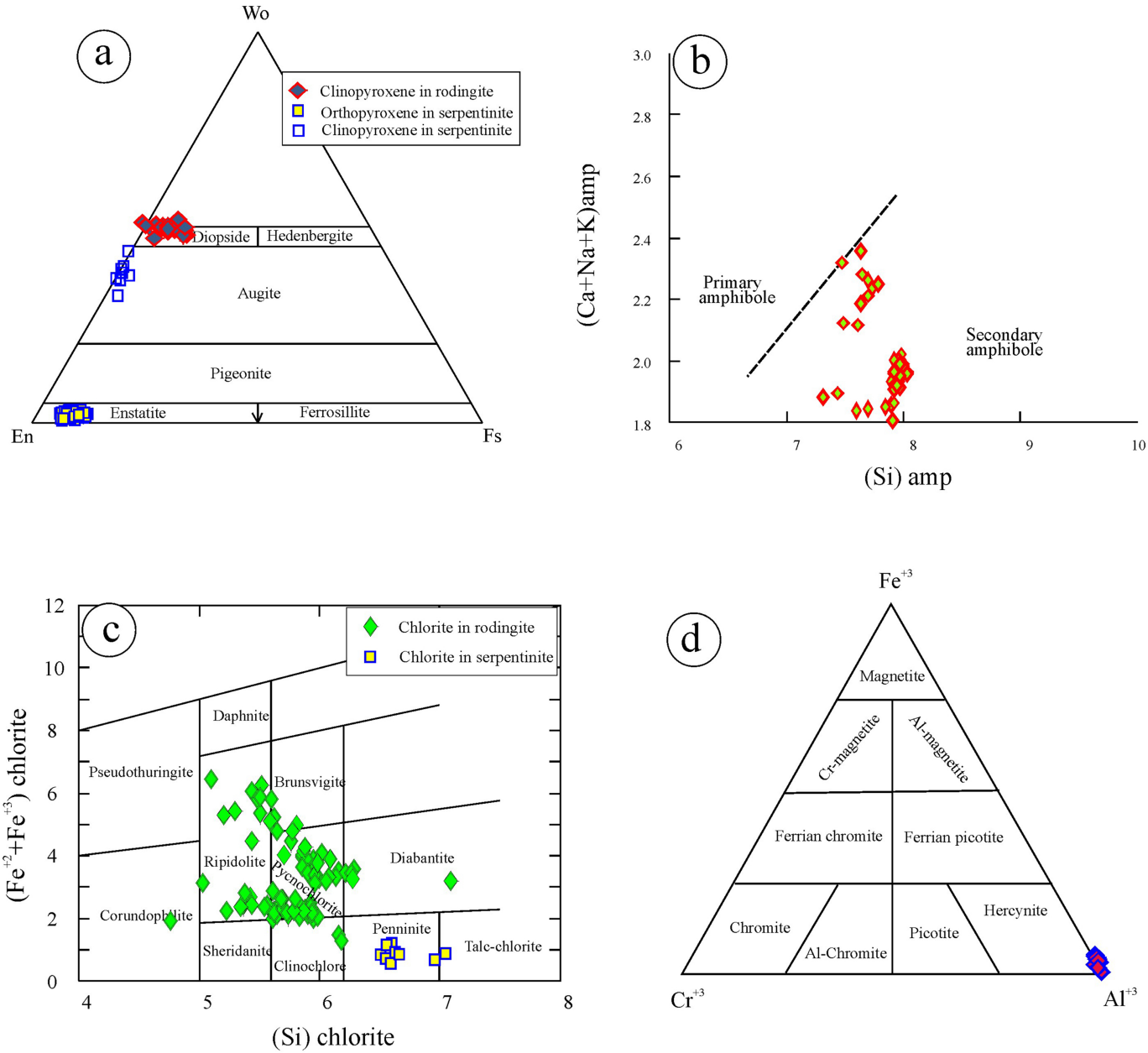
a
Wo
En
Fs
Clinopyroxene in rodingite
Orthopyroxene in serpentinite
Clinopyroxene in serpentinite
Diopside
Hedenbergite
Augite
Pigeonite
Enstatite
Ferrosillite
b
(Ca+Na+K)amp
(Si) amp
Primary amphibole
Secondary amphibole
c
(Fe+2+Fe+3) chlorite
(Si) chlorite
Chlorite in rodingite
Chlorite in serpentinite
Daphnite
Pseudothuringite
Brunsvigite
Ripidolite
Pycnochlorite
Diabantite
Corundophillite
Sheridanite
Clinochlore
Penninite
Talc-chlorite
d
Fe+3
Cr+3
Al+3
Magnetite
Cr-magnetite
Al-magnetite
Ferrian chromite
Ferrian picotite
Chromite
Al-Chromite
Picotite
Hercynite

Figure 7

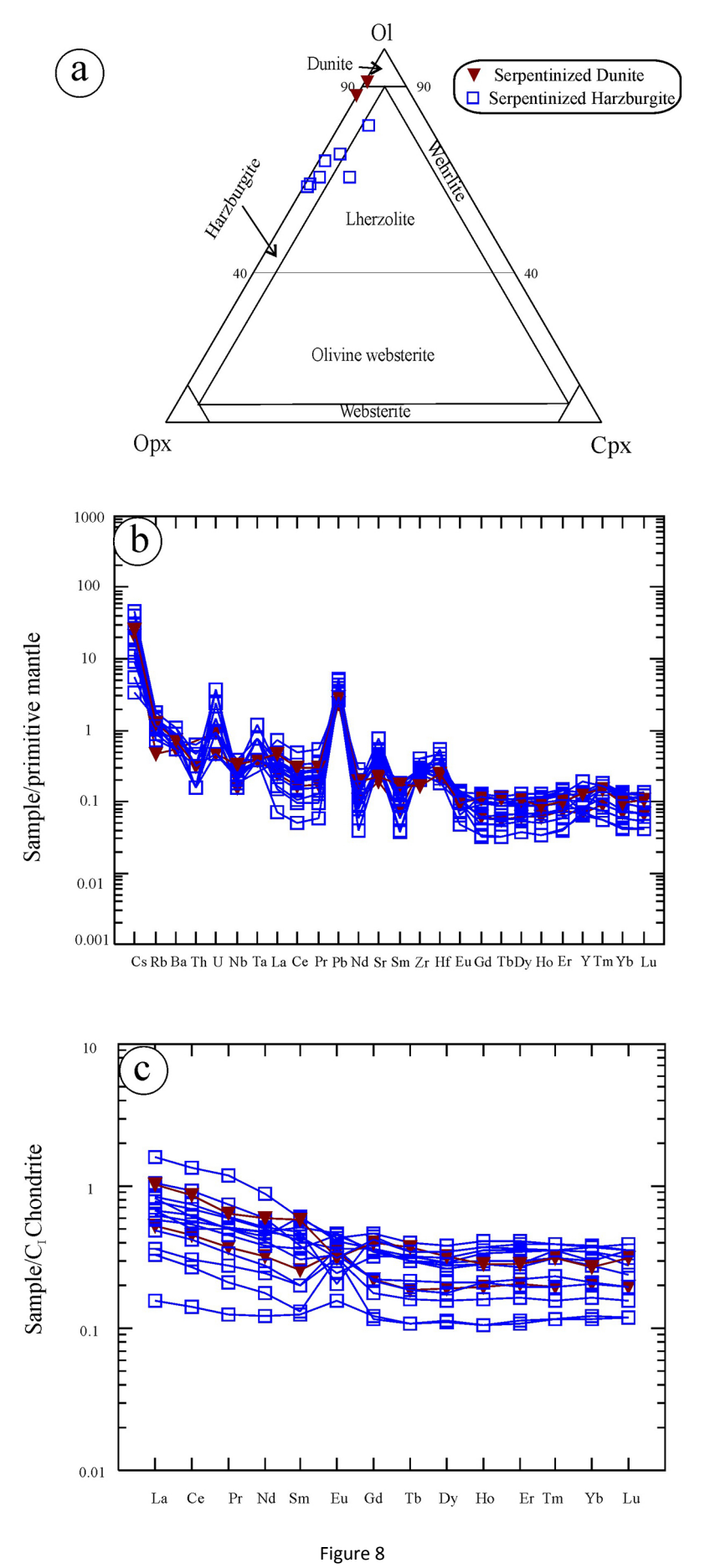
a
Ol
Dunite
90
90
Serpentinized Dunite
Serpentinized Harzburgite
Harzburgite
Wehrlite
Lherzolite
40
40
Olivine websterite
Websterite
Opx
Cpx
b
Sample/primitive mantle
1000
100
10
1
0.1
0.01
0.001
Cs Rb Ba Th U Nb Ta La Ce Pr Pb Nd Sr Sm Zr Hf Eu Gd Tb Dy Ho Er Y Tm Yb Lu
c
Sample/C1 Chondrite
10
1
0.1
0.01
La Ce Pr Nd Sm Eu Gd Tb Dy Ho Er Tm Yb Lu

Figure 8

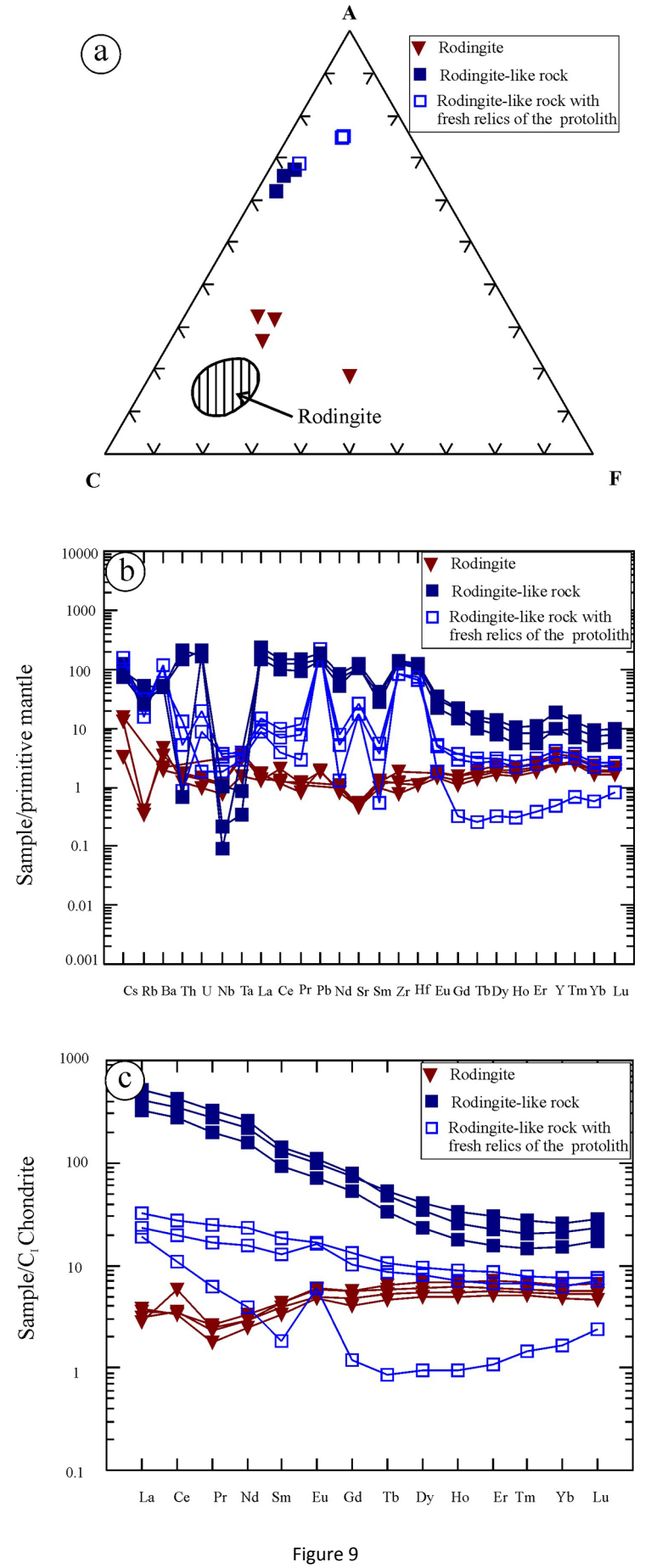
a
A
C
F
Rodingite
Rodingite-like rock
Rodingite-like rock with fresh relics of the protolith
Rodingite
b
Sample/primitive mantle
10000
1000
100
10
1
0.1
0.01
0.001
Cs Rb Ba Th U Nb Ta La Ce Pr Pb Nd Sr Sm Zr Hf Eu Gd Tb Dy Ho Er Y Tm Yb Lu
Rodingite
Rodingite-like rock
Rodingite-like rock with fresh relics of the protolith
c
Sample/C1 Chondrite
1000
100
10
1
0.1
La Ce Pr Nd Sm Eu Gd Tb Dy Ho Er Tm Yb Lu
Rodingite
Rodingite-like rock
Rodingite-like rock with fresh relics of the protolith

Figure 9

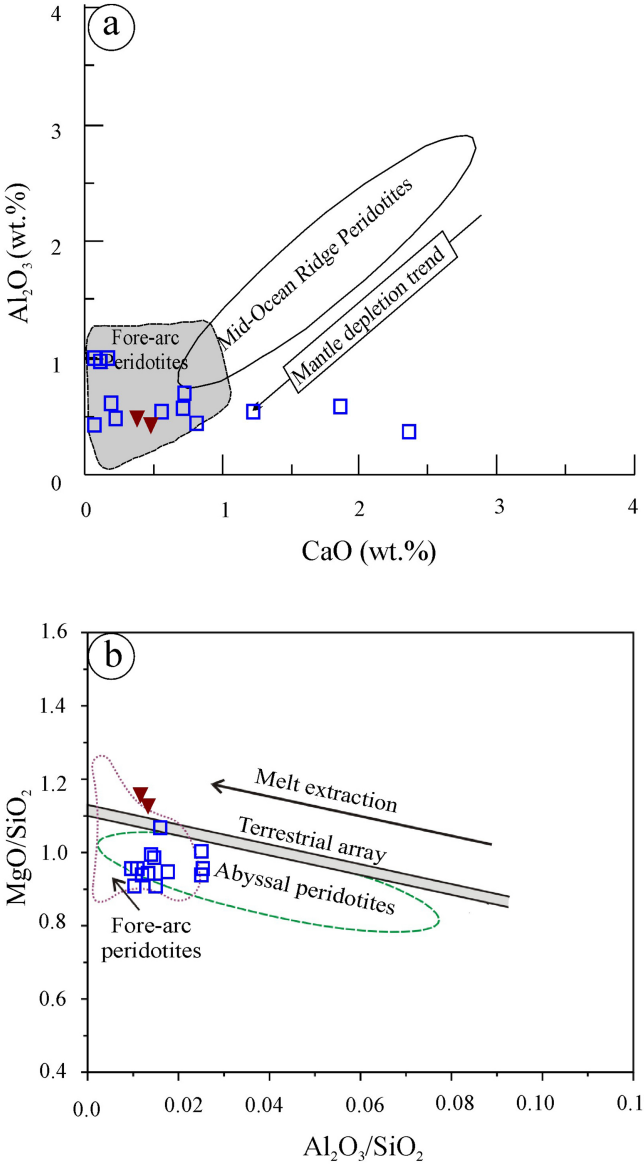
a
Al2O3 (wt.%)
CaO (wt.%)
Fore-arc peridotites
Mid-Ocean Ridge Peridotites
Mantle depletion trend
b
MgO/SiO2
Al2O3/SiO2
Melt extraction
Terrestrial array
Abyssal peridotites
Fore-arc peridotites

Figure 10

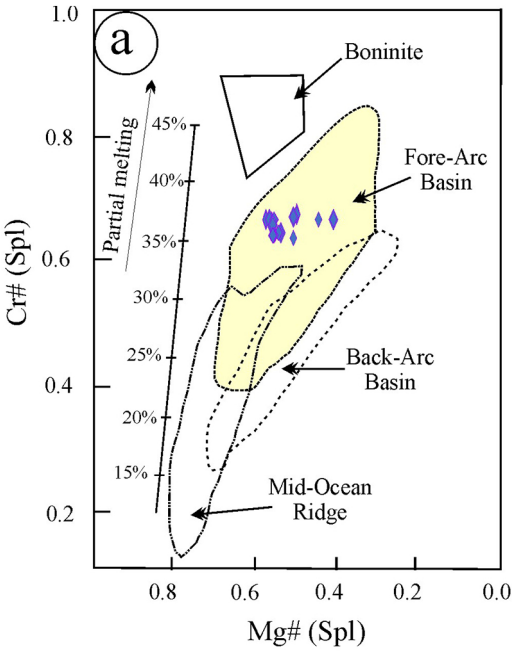
a
Boninite
Fore-Arc Basin
Back-Arc Basin
Mid-Ocean Ridge
Partial melting
45%
40%
35%
30%
25%
20%
15%
Cr# (Spl)
Mg# (Spl)
1.0
0.8
0.6
0.4
0.2
0.0

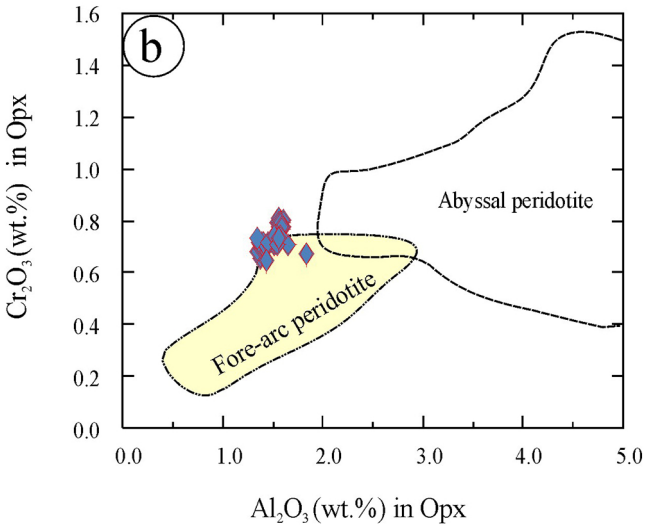
b
Abyssal peridotite
Fore-arc peridotite
Cr_2O_3 (wt.%) in Opx
Al_2O_3 (wt.%) in Opx
1.6
1.4
1.2
1.0
0.8
0.6
0.4
0.2
0.0
0.0
1.0
2.0
3.0
4.0
5.0

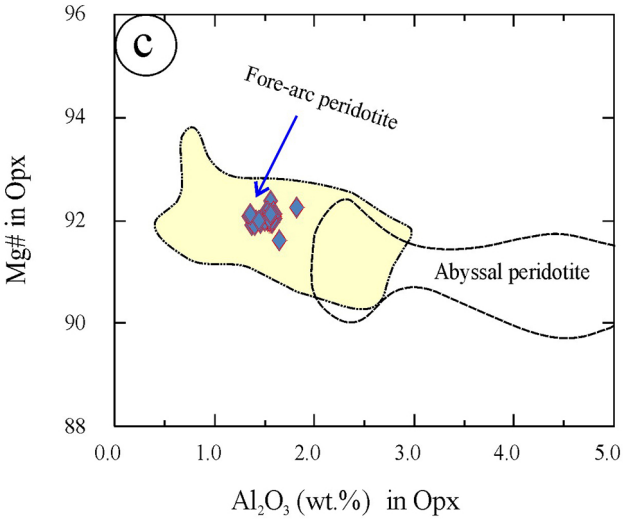
c
Fore-arc peridotite
Abyssal peridotite
Mg# in Opx
Al_2O_3 (wt.%) in Opx
96
94
92
90
88
0.0
1.0
2.0
3.0
4.0
5.0

Figure 11

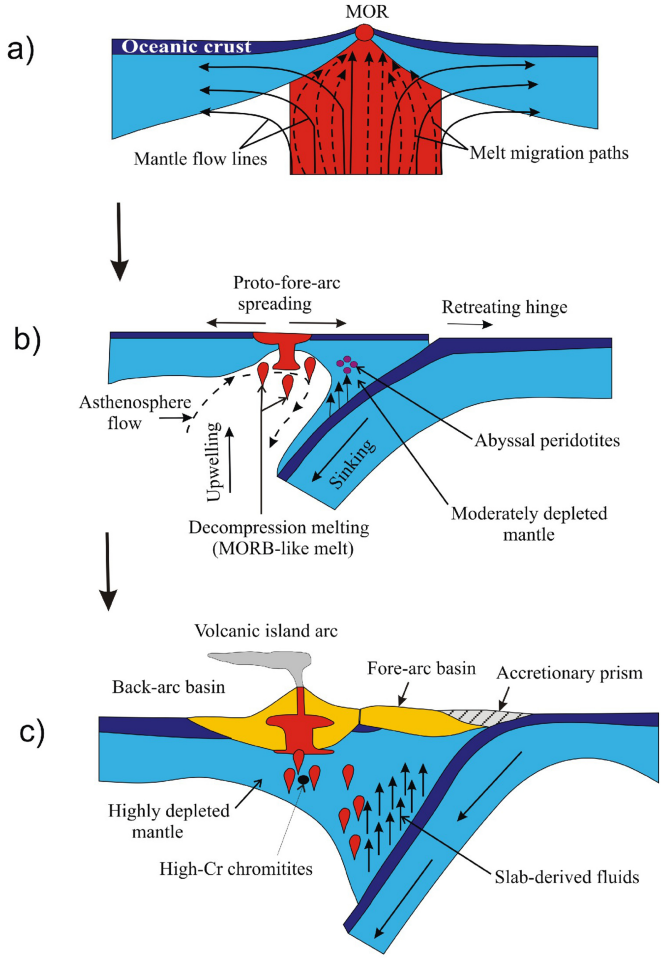
a)
MOR
Oceanic crust
Mantle flow lines
Melt migration paths
b)
Proto-fore-arc spreading
Retreating hinge
Asthenosphere flow
Upwelling
Sinking
Abyssal peridotites
Moderately depleted mantle
Decompression melting (MORB-like melt)
c)
Volcanic island arc
Back-arc basin
Fore-arc basin
Accretionary prism
Highly depleted mantle
High-Cr chromitites
Slab-derived fluids

Figure 12